CONFIDENTIAL

NAA-SR-11911
COPY
62 PAGES

UNCLASSIFIED

STATIC CONTROL OF SNAP REACTORS

(Title Unclassified)

AEC Research and Development Report

~~RESTRICTED DATA~~

This document contains restricted data as defined in the Atomic Energy Act of 1954. Its transmittal or the disclosure of its contents in any manner to an unauthorized person is prohibited.

This document contains Confidential-Restricted Data relating to civilian applications of atomic energy.

GROUP 1
Excluded from automatic downgrading and declassification

ATOMICS INTERNATIONAL
A DIVISION OF NORTH AMERICAN AVIATION, INC.

CONFIDENTIAL

DISCLAIMER

Printed in USA Price $1.30 Available from the

U.S. Atomic Energy Commission,
Division of Technical Information Extension,
P. O. Box 62
Oak Ridge, Tennessee.

Please direct to the same address inquiries covering the procurement of other classified AEC reports.

NAA-SR-11911
SNAP REACTOR,
SNAP PROGRAM
M-3679 (44th Ed.)

STATIC CONTROL OF SNAP REACTORS

(Title Unclassified)

K. R. BIRNEY
D. J. McGOFF

ATOMICS INTERNATIONAL
A DIVISION OF NORTH AMERICAN AVIATION, INC.
P.O. BOX 309 CANOGA PARK, CALIFORNIA

CONTRACT: AT(11-1)-GEN-8
ISSUED: MAY 30, 1966

DISTRIBUTION

SYSTEMS FOR NUCLEAR AUXILIARY POWER
(SNAP)-REACTOR SNAP PROGRAM
M-3679 (44th Ed.)

	No. of Copies
AEC Patent Office	1
Aerojet-General Corporation (NASA)	6
Aerojet-General Corporation, Sacramento	1
Aerojet-General Nucleonics (NASA)	1
Aeronautical Systems Division	2
Aerospace Corporation	1
Air Force Foreign Technology Division	1
Air Force Headquarters	1
Air Force Surgeon General	1
Air Force Technical Applications Center	1
Air Force Weapons Laboratory	3
Air University Library	1
AiResearch Manufacturing Company, Pheonix	1
Allison Division-GMC	1
Argonne National Laboratory	1
Army Ballistic Research Laboratories	1
Army Director of Transportation	1
ARO, Inc.	1
Battelle Memorial Institute	1
Battelle-Northwest	2
Bendix Corporation (NASA)	1
Brookhaven National Laboratory	1
Bureau of Naval Weapons	2
Bureau of Ships	2
California Patent Group	1
Central Intelligence Agency	1
Chicago Patent Group	1
Director of Defense Research and Engineering (OAP)	1
Douglas Aircraft Company, Inc., Newport Beach	1
DuPont Company, Aiken	1
DuPont Company, Wilmington	1
Electro-Optical Systems, Inc.	1
General Atomic Division	1
General Dynamics/Convair (AF)	1
General Dynamics/Fort Worth	1
General Electric Company, Cincinnati	1
General Electric Company (FPD)	2
General Electric Company (MSVD)	1
General Electric Company, San Jose	2
Hughes Research Laboratories	1
Institute for Defense Analyses	1
Jet Propulsion Laboratory	2
Johns Hopkins University (APL)	1
Lockheed-Georgia Company	1
Los Alamos Scientific Laboratory	1
Minnesota Mining and Manufacturing Company	1
Monsanto Research Company	1
Mound Laboratory	1
NASA Ames Research Center	1
NASA Goddard Space Flight Center	2
NASA Lewis Research Center	7
NASA Manned Spacecraft Center	1
NASA Marshall Space Flight Center	3
NASA Scientific and Technical Information Facility	3
National Aeronautics and Space Administration, Washington	2
National Reactor Testing Station (PPCO)	4
Naval Air Development Center	1
Naval Radiological Defense Laboratory	1
Naval Research Laboratory	2
Navy Marine Engineering Laboratory	1
New York Operations Office	1
Nuclear Weapons Training Center Pacific	1
Oak Ridge Operations Office	1
Office of Naval Research	2
Office of the Chief of Engineers	1
Office of the Chief of Naval Operations	3
Office of the Chief of Naval Operations (OP-03EG)	2
Pratt and Whitney Aircraft Division (NASA)	1
Rand Corporation	1
Radio Corporation of America	1
Sandia Corporation	1
Union Carbide Corporation (ORNL)	8
United Nuclear Corporation (NDA)	1
University of California, Livermore	1
Westinghouse Electric Corporation, Lima	1
Westinghouse Electric Corporation, Lima (AF)	1
Westinghouse Electric Corporation (NASA)	1
Westinghouse Electric Corporation (WAL)	1
White Sands Missile Range	2
Division of Technical Information Extension	10
AI Library (Includes 2 copies to CPAO, 2 copies to AEC, Washington, 2 copies to COO)	44

ACKNOWLEDGMENT

The authors are indebted to R. A. Johnson who provided much of the information concerning SNAP reactor operating experience contained in this report. Valuable technical assistance was provided by many people, notably J. P. Hawley, L. D. Swenson, A. R. Fallon, and E. M. Faelten.

CONTENTS

CONTENTS

TABLES

FIGURES

FIGURES

ABSTRACT

The control of a nuclear reactor in space presents problems for any mechanical system which may be used, especially for the long lifetimes (3 to 5 years) being considered. The concept of static control (no moving parts after a short active control period) has been investigated to determine the feasibility of this method of control. Since reliability of the power source for any space application is of the utmost importance, static control allows a high reliability by eliminating the control system failure probability.

The selection of a reactor temperature-time profile and the uncertainties associated with maintaining it during operation are estimated. For a given power range a prepoison may be selected to supply the required reactivity gain. Hydrogen leakage, which is strongly temperature dependent, serves to damp the swing in reactor temperature with time. The nominal design considered is for a 50°F maximum temperature swing during the operating life under static control. If the temperature rises due to a miscalculation of reactivity change rates, hydrogen leakage increases and tends to reduce temperatures, hence significantly decreasing the temperature rise. The opposite effect occurs when the temperature falls. This effect is unique with metal-hydride moderated reactors.

A potentially attractive design approach would be to design and prepoison the reactor for operation under static control and employ an active control system. This mode of operation would minimize the consequences of a failure in the mechanical control system and decrease the temperature swing established for static control operation. Such a system would have the capability of following load requirements and, during its active lifetime, would not be limited to nearly constant power operation.

This study concludes that the use of static control for the control of SNAP reactors appears to be an attractive mode of operation at core outlet temperatures up to 1300°F with improved hydrogen leakage barriers. The barrier material used for SNAP 10A and SNAP 8 Experimental Reactor (S8ER) is suitable at core outlet temperatures up to 1200°F and the hydrogen barrier for SNAP 8 Developmental System (S8DS) has met the acceptance test requirements

at 1400°F, isothermal. Long-term endurance tests (out of core, isothermal) indicate that hydrogen leakage is sufficiently low that static control is feasible at 1300°F outlet temperature for lifetimes up to 2 years and power levels approaching 300 thermal kilowatts.

I. INTRODUCTION

The SNAP 10-SNAP 8 family of compact nuclear reactors has been developed by Atomics International under contract with the U.S. Atomic Energy Commission to provide a long-lived energy source for electric power generation in space. These reactors have been designed for remote, completely automatic startup and unattended long-term operation.

The cores of SNAP reactors consist of uranium-zirconium alloy fuel elements clad in Hastelloy-N. The uranium is fully enriched in U^{235} and comprises 10% by weight of the fuel. The fuel material is hydrided to an N_H of 6.0 to 6.4 $\times 10^{22}$ atoms of hydrogen/cc with the result that the moderator is intimately mixed with the fuel. Use of zirconium hydride permits a hydrogen density approaching that of cold water with a dissociation pressure, at 1200°F, less than one atmosphere.(1)

The fuel elements are arranged in a triangular array and are positioned and constrained in the core by upper and lower grid plates. The reactor is cooled by NaK-78, an eutectic mixture of sodium and potassium, and the core is reflected radially by beryllium.

Because of the small size of the reactor, a large fraction of the neutrons born in the reactor leaks from the core and permits the use of leakage changes for both coarse and fine control. In this concept segments of the reflector are moved to provide streaming paths for neutrons emerging from the core. The resulting changes in leakage cause a reduction in reactivity of the reactor.

The SNAP 10A reactor is shown in Figure 1 as an example of SNAP reactor geometry. The reactor contains 37 fuel elements and is controlled by 4 semicylindrical control drums. In this design a thermoelectric pump is mounted on the outlet coolant line. A shadow shield is mounted below the reactor to attenuate the radiation emitted in the direction of the payload.

SNAP reactors can be used as a heat source with a variety of power conversion systems for the production of electrical power. The thermoelectric power conversion system, used in the SNAP 10A flight systems, is shown in Figure 2. Hot NaK is pumped from the reactor downward through 40 tubes in the power

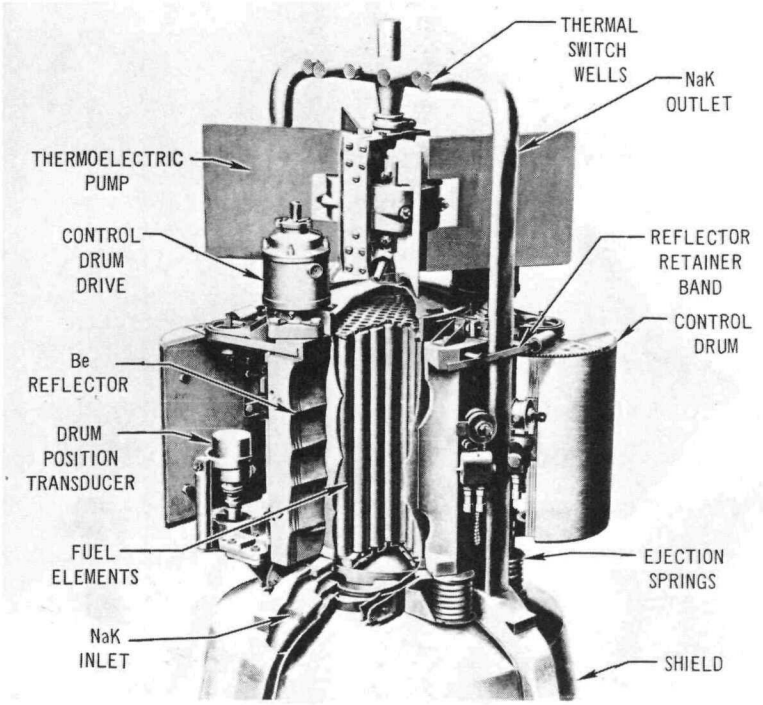

2-5-65 7580-10512D

Figure 1. SNAP 10A Reactor

conversion system to a lower manifold where it is collected and returned to the reactor. Attached to each of the tubes are 72 silicon-germanium thermocouples which provide approximately 550 watts(e) of power when operating at the nominal outlet temperature of 1020°F. Thermoelectric conversion modules are now available which will operate at significantly higher outlet coolant temperatures up to ~1300°F.

Other power conversion systems, such as mercury-Rankine and Brayton cycle systems, can also be satisfactorily mated with SNAP reactors.

Five reactors have been operated as part of the SNAP development program. The first was the SNAP Experimental Reactor (SER), which began operation in the spring of 1959 and produced 225,000 kwh of energy prior to its scheduled shutdown in 1960. This reactor demonstrated the feasibility of the zirconium-hydride concept and provided the first data on reactivity losses during operation.

The second SNAP reactor was the SNAP Developmental Reactor (SDR), which operated between April 1961 and December 1962 logging over 11,300 test hours.

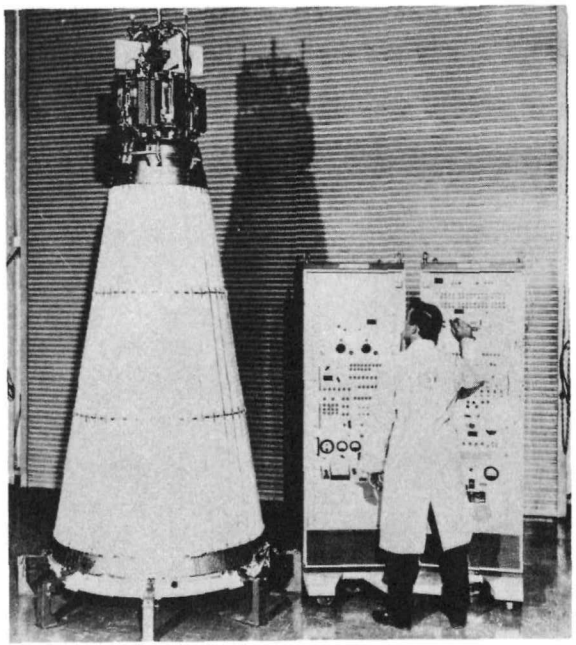

8-11-65

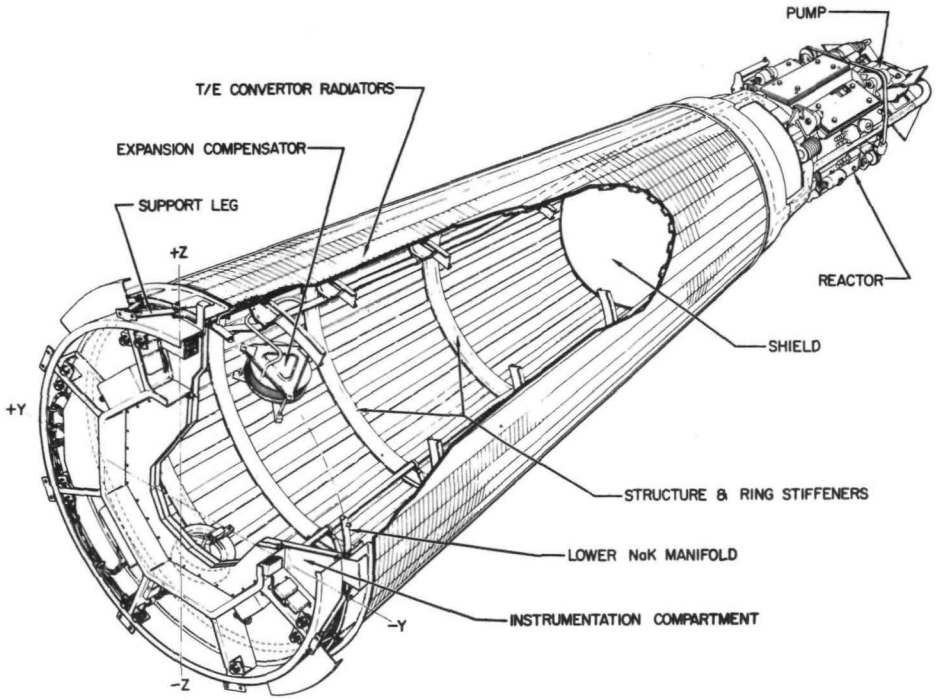

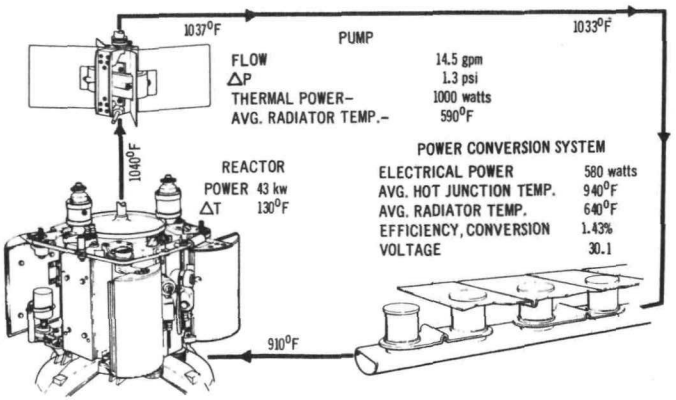

7561-02857

Figure 2. SNAP 10A System

The fuel-moderator elements in this reactor were generally of the configuration used in later SNAP reactors. The hydrogen redistribution reactivity loss mechanism was first recognized in this reactor and the effect of hydrogen loss was observed at various temperatures. These are the two reactivity loss mechanisms which are unique to the SNAP zirconium-hydride type reactors.

Verification of the SNAP reactor capability at higher temperatures and power was obtained from the recent operation of the actively controlled S8ER. During its test program, S8ER accumulated a total of 10,320 operating hours at 400 kwt, or more, of which 8,800 hours were at coolant outlet temperatures of 1300°F. Additional data on hydrogen redistribution, hydrogen loss, and other reactivity loss mechanisms were obtained from experiments performed using this reactor.

Use of the static control mode of operation allows power production for periods of 1 to 5 yr with no mechanical movement of any reactor component after a short initial reactor stabilization period. Reactivity insertion due to the burnout of an initially loaded prepoison is used to compensate for operating reactivity losses. The small reactivity mismatch causes a slight temperature drift; the magnitude of the drift is governed by the negative temperature coefficient of the reactor. The lack of any control system movement after the initial stabilization period enables operation of the reactor with no moving parts. If the reactor is then used with a static power conversion system, such as a thermoelectric system, electric power is generated with no moving parts in the entire system. This can be of great benefit for remote operation applications.

Two SNAP 10A reactors have been operated under the static control mode of operation. The performance of these reactors will be discussed in a following section. The two reactors are identical; one was operated in orbit, while the other has completed 10,000 hr of simulated space operation at the Santa Susana Test Site in California.

This report deals with the feasibility of static control and the problems associated with its application to SNAP reactor systems. The problems of prepoisoning and the influence of poison selection on the time behavior of the reactor have been determined. The effects of uncertainties in reactivity predictions and

the resulting uncertainties in reactor temperature have been examined and found to be manageable. Though the report discusses the application of statically-controlled reactors to thermoelectric systems, the results developed are almost entirely applicable to other systems.

II. SNAP REACTOR REACTIVITY LOSSES

SNAP reactor reactivity losses can be classified as short-term ("saturating") losses or as long-term ("operational") losses. The magnitude of the short-term losses is essentially independent of the operating life of the reactor and depends only on reactor power, temperature, and configuration. The long-term losses continue throughout reactor operation and therefore also depend on the lifetime of the reactor.

A. SHORT-TERM REACTIVITY LOSSES

1. Temperature and Power Defects

As the temperature of a SNAP reactor is increased above ambient, a loss in reactivity occurs. Thermal expansion of the core vessel and reflector components results in a reduction in effective density and an increase in neutron leakage. An isothermal temperature coefficient may be determined by non-nuclear heating of the reactor. The operating reactor is not isothermal, and a power coefficient is used to account for the reactivity changes from isothermal conditions. It is calculated by the equation:

$$\alpha_p = \sum_i \alpha_{T,i} \left(d\hat{T}_i/dP\right)$$

where

α_p = power coefficient ($\not{c}$/kw),

$\alpha_{T,i}$ = "partial" temperature coefficient for component i ($\not{c}$/°F), and

$\left(\frac{d\hat{T}_i}{dP}\right)$ = change in temperature of component i per unit change in reactor power averaged in an importance sense.

The summation is taken over such reactor components as the fuel, grid plates, and reflector. The power coefficient is a rather strong function of reactor core configuration since, for example, the temperature rise (centerline-to-edge) across the fuel per unit power depends to a high degree on the fuel element size. The isothermal coefficient is a much weaker function of the core configuration, depending primarily on the gross reactor leakage, the neutron spectrum, reflector configuration, and prepoison loading.

The SDR isothermal temperature coefficient was experimentally determined using both period measurements and a calibrated control drum. Both methods showed a coefficient of -0.21¢/°F from ambient temperature to 800°F. Above 800°F the coefficient increases and is near -0.3¢/°F at 1100°F.[2]

No reason for the increase in magnitude above 800°F was given in the original analysis. Speculation included the fuel spectral effect or thermomechanical "seating in" of some component. The scatter observed at temperatures as low as 600°F indicates that the trend may be a more gradual, perhaps even linear, increase with temperature.

The isothermal temperature coefficient for S8ER was measured[3] at 50°F intervals with the core average NaK temperature ranging from 300 to 1250°F. The measurements were obtained by use of both "positive period measurements" and "level position" methods.

The positive period measurement method used identical drum positions at two successive temperatures to produce positive periods. The temperature defect was determined for the temperature change from the difference in the periods. This method is considered more accurate than the level position method which determined the temperature defect by the difference in control drum positions at "exactly critical" for two successive temperatures. The difficulties with the level position method stem from determining the exactly critical position and from the uncertainty in the control drum calibration. The level position measurements confirmed the positive period measurement analysis. The results of the experiments are shown in Table 1.

TABLE 1

MEASURED ISOTHERMAL TEMPERATURE COEFFICIENTS FOR S8ER

Temperature (°F)	Experimental Results (¢/°F ± 0.01)
300	-0.16
800	-0.18
1200	-0.20

2. Hydrogen Redistribution

Hydrogen migrates within fuel elements under the influence of temperature gradients. The net flow from hotter to colder portions of the fuel rod continues until a quasi-equilibrium state of spatially-constant hydrogen partial pressure within each fuel element is reached. This state is at best one only of quasi-equilibrium since the hydrogen inventory is continuously decreasing due to leakage from the elements. Since the net flow of hydrogen is to the colder portions of the fuel rod, and since these regions are in general regions of lower nuclear worth, a net reactivity loss results.

Hydrogen redistribution experiments have been performed on the SDR, S8ER, and S10FS-3 reactors. Hydrogen redistribution reactivity loss appears to saturate with a temperature-dependent time constant and, in simplest form, may be expressed as,

$$\Delta\rho_{HR}(t) = \Delta\rho_{HR}(\infty)[1 - e^{-t/\tau}]$$

where

$\Delta\rho_{HR}(t)$ = reactivity loss due to redistribution at time t,

$\Delta\rho_{HR}(\infty)$ = equilibrium redistribution reactivity loss, and

τ = time constant for redistribution.

Measured time constants are shown in Figure 3 together with estimated uncertainty limits.

The reactivity worth of equilibrium hydrogen redistribution, for constant inlet temperature, increases as the power increases and as the core ΔT is increased. At constant power and constant core ΔT the worth increases as the inlet temperature is reduced.

3. Xenon Buildup

Because of its large thermal absorption cross-section ($\sim 3 \times 10^6$ barns), xenon-135 is the most significant fission product poison formed. It is formed primarily by the radioactive decay of tellurium-135, as shown in the following decay chain: $Te^{135} \xrightarrow{1\ min} I^{135} \xrightarrow{6.7\ hr} Xe^{135} \xrightarrow{9.2\ hr} Cs^{135} \xrightarrow{2.1 \times 10^6\ yr} Ba^{135}$. Since the half-life of tellurium-135 is of such short duration, the analysis is simplified by assuming that iodine-135 is produced directly from fission. The

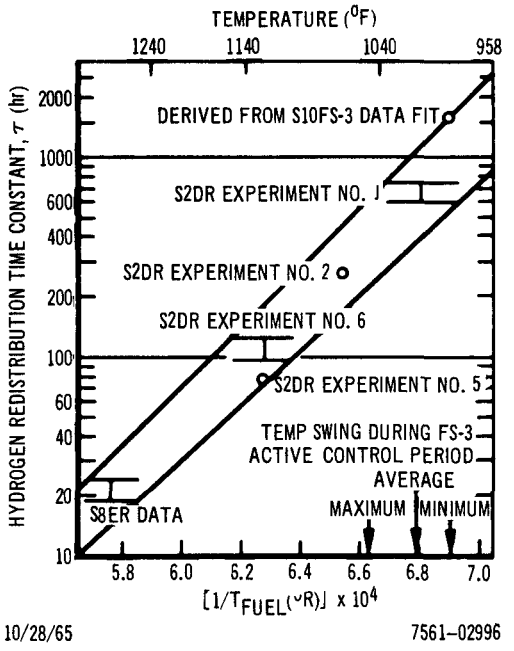

Figure 3. Hydrogen Redistribution Time Constant vs Average Fuel Temperature

concentration of xenon is therefore governed by the following differential equations.

$$\frac{dI}{dt} = \Sigma_f \varphi \gamma_I - \lambda_I I$$

$$\frac{dX}{dt} = \lambda_I I - (\sigma_x \varphi + \lambda_x) X + \Sigma_f \varphi \gamma_x$$

where

I = iodine-135 concentration

Σ_f = macroscopic U^{235} fission cross section

φ = neutron flux

γ_I = iodine-135 yield from fission

γ_x = xenon-135 yield from fission

λ_I = iodine decay constant

X = xenon-135 concentration

σ_x = microscopic xenon-135 absorption cross section

λ_x = xenon-135 decay constant

It is assumed that burnout of iodine by neutron absorption is negligible compared to its removal by radioactive decay. The flux used in the calculations is the total flux, integrated over energy, and the cross sections are one-group cross sections averaged over the entire energy spectrum. Because of this method of energy-averaging, the cross sections are much smaller than would be obtained by thermal-flux weighting, but the integrated reaction rate is identical.

If the steady-state condition is specified (derivatives set equal to zero), the equilibrium concentration of xenon is obtained as,

$$X_{\infty} = \frac{(\gamma_I + \gamma_x)\Sigma_f \varphi}{\lambda_x + \sigma_x \varphi}$$

From Reference 4:

$\gamma_I = 0.056$

$\gamma_x = 0.003$

$\lambda_I = 2.87 \times 10^{-5}$ sec^{-1}

$\lambda_x = 2.09 \times 10^{-5}$ sec^{-1}.

For the spectrum and loading of a SNAP 10A reactor,

$\Sigma_f = 0.02689$ cm^{-1}

$\sigma_x = 2.322 \times 10^5$ barns.

The equilibrium worth of xenon is a function of the uranium-235 loading and the flux level. The model gives a xenon coefficient of -0.39¢/kw for SNAP 10A and -0.23¢/kw for S8ER.

For the low flux levels ($\sim 10^{12}$ n/cm^2-sec) encountered in SNAP 10A reactor operation, the burnout of xenon by absorption ($\sigma_x \varphi$) is negligible compared to radioactive decay (λ_x) hence no xenon override capability is required. Under these circumstances the equilibrium concentration, and therefore the equilibrium worth, is proportional to reactor power. From S8DR experiments, this constant of proportionality has been determined to be -0.41¢/kw.* For different loadings, spectra, and higher power levels, the concentration must be calculated.

*1 cent = 0.01 dollar = 0.00008 Δk/k.

The reactivity effects of xenon poisoning were measured in the larger SNAP 8 reactor[3] by monitoring the change in excess reactivity caused by a rapid change in steady-state power levels. The power changes were made at conditions such that the transient reactivity effects caused by hydrogen redistribution and temperature changes were minimized. The change in excess reactivity was corrected to account for reactivity effects which could not be eliminated by experimental technique. The ±7% uncertainty in the measurement is mainly attributed to the uncertainty in the absolute power measurement. The xenon worth at 600 kw was determined to be \$1.26 ± 0.09, or -0.21¢/kw.

B. LONG-TERM REACTIVITY EFFECTS

1. Fission Product Buildup

A continuing source of reactivity depletion is the formation of fission fragments possessing large absorption cross sections. These poisons are classified as rapidly-saturating, slowly-saturating, or non-saturating, depending on the extent to which they build up to steady-state concentrations under SNAP reactor operating conditions. Contributions from each of these groups were summed to provide a total fission product cross section (barns/fission) as a function of exposure. Because of its very rapid saturating nature, samarium-149 is treated as a separate poison. Cross sections obtained in this manner are presented in Table 2.

2. Fuel Depletion

Because of the low moderator to fuel ratio in SNAP reactors, the incremental worth of fuel is very small. For the small quantities burned out in SNAP 10A operation, for example, the reactivity loss rate is linear with burnout and has been calculated to be -9.1¢/% U^{235}.

3. Hydrogen Loss

At operating temperatures, the internal hydrogen pressure causes hydrogen permeation through the cladding tubes into the NaK coolant. It then leaks through the core vessel walls and system piping and is lost. Environmental reactivity calculations and critical experiments indicate that the worth of leaking hydrogen is about \$1.00/0.1 N_H unit. To inhibit the rate of leakage a ceramic hydrogen barrier is applied to the inside of the cladding tubes. Permeation through this

TABLE 2

FISSION PRODUCT CROSS SECTIONS FOR SNAP 10A REACTORS
(For use with the SIZZLE code)
(Xe^{135} and Sm^{149} not included)

Energy Increment	Energy Group	Exposure (kwt x year)		
		0	100	1000
		Cross Sections (barns/fission)		
0.1 Mev to 10 Mev	1 through 5	0	0	0
17 kev to 0.1 Mev	6	0.11	0.11	0.11
3 kev to 17 kev	7	0.55	0.55	0.54
550 ev to 3 kev	8	1.45	1.44	1.40
100 ev to 550 ev	9	7.79	7.78	7.55
30 ev to 100 ev	10	19.5	19.4	18.8
10 ev to 30 ev	11	21.0	21.0	20.1
3 ev to 10 ev	12	68.3	68.2	63.3
1 ev to 3 ev	13	24.7	24.5	22.5
0.4 ev to 1 ev	14	15.0	14.9	13.9
0.1 ev to 0.4 ev	15	25.1	23.8	19.7
0.001 ev to 0.1 ev	16	89.4	81.8	59.1

barrier (and defects in the barrier) becomes the limiting loss rate-determining mechanism.

The equation describing the permeation through the barrier is,

$$L = K_1 P^{1/2} e^{-K_2/T} + \frac{K_3 P T^{5/2} e^{-K_4/T}}{T^{5/2} + K_5 P e^{-K_4/T}}$$

where

L = hydrogen leakage current from element surface ($cc/hr\text{-}cm^2$)

T = local temperature of barrier (°R)

P = hydrogen pressure inside element (atm), and

K_1, K_2, K_3, K_4 = constants depending upon nature of coating and application process.

For the SNAP 10A elements,

$$K_1 = 1.42 \text{ cc/hr-cm}^2\text{-atm}^{1/2}$$

$$K_2 = 12{,}760/^\circ\text{R}$$

$$K_3 = 4{,}554 \text{ cc/hr-cm}^2\text{-atm}$$

$$K_4 = 28{,}160/^\circ\text{R, and}$$

$$K_5 = 8.432 \times 10^{13} (^\circ\text{R})^{5/2}/\text{ atm.}$$

Hydrogen leakage is strongly temperature-dependent, essentially doubling with a 50°F increase in temperature. The rate of hydrogen leakage also decreases rapidly with depletion of hydrogen as the hydrogen concentration, and therefore the hydrogen pressure driving force, decreases.

All the reactivity effects mentioned above, short- and long-term, are reactivity loss mechanisms. To compensate for these losses, a reactivity gain mechanism is needed. The burnout of an initially loaded prepoison fulfills this requirement and is described in the next section.

4. Prepoison Burnup

Several prepoison materials have been considered for use, but the equations that follow are for samarium-149. The long-term effects include the burn-in of samarium-149, unless the effect is reversed by preloading greater than the equilibrium concentration in the core. The equations relating samarium-149 concentration with time may be derived as follows.

Neodymium-149 is a direct fission product which decays to promethium-149 which decays to samarium-149, a stable isotope ($\sim 10^{14}$ year half life).

$$Nd^{149} \xrightarrow{2.0h} Pm^{149} \xrightarrow{53h} Sm^{149} ,$$

$$dN + \lambda N dt = \gamma \Sigma_f \varphi dt, \text{ and}$$

$$N = \frac{\gamma \Sigma_f \varphi}{\lambda_n} (1 - e^{-\lambda_n t}) \quad .$$

after $\sim$10 hours, $$N = \gamma \Sigma_f \varphi / \lambda_n \quad ,$$

$$dP + \lambda_p P dt = \lambda_n N dt \quad ,$$

$$dP + \lambda_p P dt = \gamma \Sigma_f \varphi dt \quad ,$$

$$P = \frac{\gamma \Sigma_f \varphi}{\lambda_p} (1 - e^{-\lambda_p t}) \quad ,$$

$$dS + (\lambda_S + \varphi\sigma) S dt = \lambda_p P dt \quad ,$$

$$\lambda_S \equiv 0$$

$$dS + \varphi\sigma S dt = \gamma \Sigma_f \varphi (1 - e^{-\lambda p t}) \, dt \quad ,$$

$$S e^{\varphi\sigma t} = \gamma \Sigma_f \varphi \int (1 - e^{-\lambda p t}) e^{\varphi\sigma t} \, dt \quad , \text{ and}$$

$$S = \frac{\gamma \Sigma_f \varphi}{\varphi\sigma(\lambda_p - \varphi\sigma)} [\lambda_p (1 - e^{-\varphi\sigma t}) - \varphi\sigma (1 - e^{-\lambda p t})] \quad .$$

Generally $\varphi\sigma << \lambda_p$ and

$$S = \frac{\gamma \Sigma_f \varphi}{\varphi\sigma} (1 - e^{-\varphi\sigma t}) \quad ,$$

$$S(t) = (\gamma\Sigma_f\varphi/\varphi\sigma)\ (1 - e^{-\varphi\sigma t}) + S(0)e^{-\varphi\sigma t} \quad ,$$

$$S(\infty) = \gamma\Sigma_f\varphi/\varphi\sigma \quad , \text{ and}$$

$$S(t) = S(\infty)\ (1 - e^{-\varphi\sigma t}) + S(0)e^{-\varphi\sigma t} \quad .$$

This equation is used to calculate the reactivity gain due to the burnout of samarium-149. Similar equations are available for other burnable poisons which might be used. The notation used here is listed below.

t = time

N = number of Nd^{149} (atoms/cc)

P = number of Pm^{149} (atoms/cc)

S = number of Sm^{149} (atoms/cc)

λ_n = decay constant for Nd^{149} ($time^{-1}$)

γ = 0.0113, yield from fission of mass ^{149} isotope,

Σ_f = macroscopic fuel cross section for U^{235} (cm^{-1})

λ_p = decay constant for Pm^{149} ($time^{-1}$)

φ = average flux (n/cm^2-sec)

σ = Sm^{149} cross section (cm^2)

$S(t)$ = Sm^{149} concentration at time t

$S(\infty)$ = Sm^{149} concentration at equilibrium

$S(0)$ = Sm^{149} concentration at time zero.

The concentration for dilute mixtures of prepoison in the core is directly proportional to the reactivity worth. Reactivity worths may be substituted directly into the equations in place of the samarium-149 concentration.

III. PREPOISON SELECTION FOR STATIC CONTROL

The choice of a particular prepoison and the concentration selected for a SNAP reactor static control application must fulfill two criteria: (1) the magnitude of the reactivity insertion due to prepoison burnout must be sufficient to compensate for the reactivity losses outlined in the preceding section, and (2) the rate of reactivity insertion must not differ significantly from the rate of reactivity losses. Any significant differences between the rates of reactivity insertion and removal will result in severe temperature drifts during lifetime even though the magnitudes of total insertion and removal are identical.

The temperature profile during lifetime, and therefore the required reactivity insertion during life, will depend on the prepoison loaded. Since the reactivity loss (primarily due to hydrogen leakage) is strongly dependent on temperature, the shape of the temperature-time profile influences the operational reactivity losses. The reactivity mismatch determines the shape of the temperature profile, and the rate of prepoison burnout varies slowly with temperature. It can be seen that there are many combinations of prepoisons which will provide a specified end-of-life reactor temperature under static control. The shape of the temperature profile during lifetime will depend on that poison loaded. Therefore, the amount of prepoison to be loaded is dependent on the poison combination chosen.

If appropriately-averaged one-group cross sections and fluxes are defined, the worth of the poison at any time follows a simple exponential law,

$$\rho_p(t) = \rho_p(0)\, e^{-\varphi\sigma_p t}$$

where

$\rho_p(t)$ = reactivity worth of poison at time t

$\rho_p(0)$ = initial reactivity worth of poison

σ_p = microscopic poison absorption cross section, and

φ = total flux in reactor

The flux, however, is given by

$$\varphi = K \frac{Q}{U\sigma_f}$$

where

Q = thermal power of reactor

U = uranium-235 loading

σ_f = uranium-235 microscopic fission cross section, and

K = proportionality constant.

Substituting for the flux,

$$\frac{\rho_p(t)}{\rho_p(0)} = e^{-K\left(\frac{Qt}{U}\right)\left(\frac{\sigma_p}{\sigma_f}\right)} \quad .$$

This equation indicates that the fractional burnout of a prepoison depends both upon the specific energy release $\left(\frac{Qt}{U}\right)$ and the ratio of the microscopic poison cross section to the microscopic fission cross section. Use of a poison with too high a microscopic cross section will lead to too rapid initial poison burnout. The associated reactivity gain rate far exceeds the reactivity loss rates accompanying reactor operation. As a result, temperature peaking accelerates hydrogen leakage. At the end of life, when the poison is substantially burned out, the reactivity loss rate exceeds the gain rate and the temperature falls rapidly. Very large temperature swings during life result. If the cross section of the prepoison is too small, too large a fraction of the prepoison will remain at the end of life. This residual poison comprises a reactivity penalty. The decision as to whether a poison cross section is too large or too small depends on the other term in the exponent, $\frac{Qt}{U}$. As this specific extracted energy increases, the desired prepoison cross section decreases. Experience has shown that, for operation of statically controlled reactors at elevated temperatures (1200 to 1300°F coolant outlet temperatures), approximately 30 to 40% of the prepoison should remain at the end of life if a reasonably flat temperature-time profile is to be obtained. (This is discussed in Appendix B.) The cross section of the poison should therefore be roughly inversely proportional to specific energy release.

Several isotopes have been studied to determine their use as prepoisons for statically-controlled SNAP reactors. Since only a few grams of material are used in most cases, the use of separated isotopes has not been avoided. The list of isotopes presented in Table 3 is not intended to be complete. Some materials not included, such as hafnium, have shown promise and their use as burnable poisons is under consideration.

TABLE 3

PREPOISONS FOR STATIC CONTROL OF SNAP REACTORS

Isotope	One-Group Absorption Cross Sections (barns)*	σ_a/σ_f*
Gadolinium-157	3600	160
Samarium-149	2500	110
Cadmium-113	1390	62
Gadolinium-155	1000	44
Europium-151	370	16.4
Boron-10	143	6.3

*Based on a 10 wt % uranium - $ZrH_{1.8}$ spectrum
σ_a is the spectrum averaged absorption cross section for each poison, σ_f is the spectrum averaged fission cross section for U^{235}.

Because of the different energy-dependencies of the various cross sections, the ratio σ_a/σ_f will shift with neutron spectrum. Only minor changes are noted with slight shifts in reactor size or hydrogen concentration. Some cross section ratios change rapidly with changes in the uranium content in the uranium-zirconium hydride fuel. The dependence of this ratio on uranium content is shown in Figure 4.

Using a 10 wt % uranium - $ZrH_{1.8}$ spectrum, the fractional poison burnout as a function of poison cross section ratio and specific energy release is shown in Figure 5. If a fractional residual poison of 30 to 40% is considered near optimum at the end of life, a range of applicability for each of the poisons in Table 3 may be obtained from Figure 5. Table 4 indicates this range of applicability.

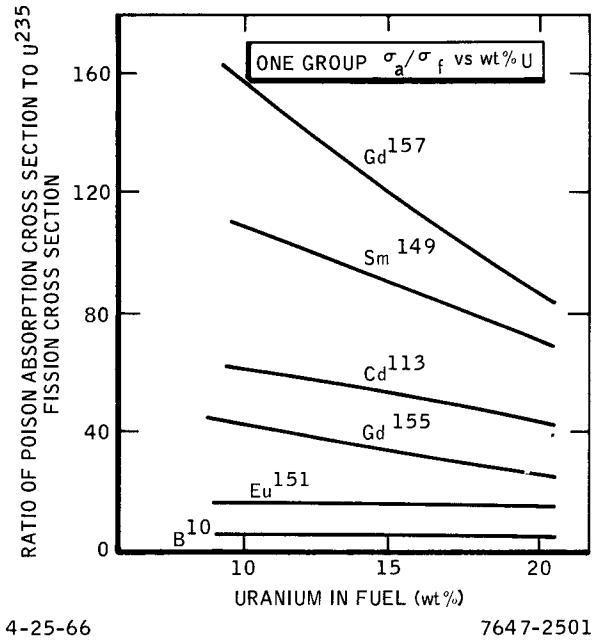

Figure 4. Absorption-to-Fission Cross Section Ratios for Possible SNAP Reactor Prepoisons

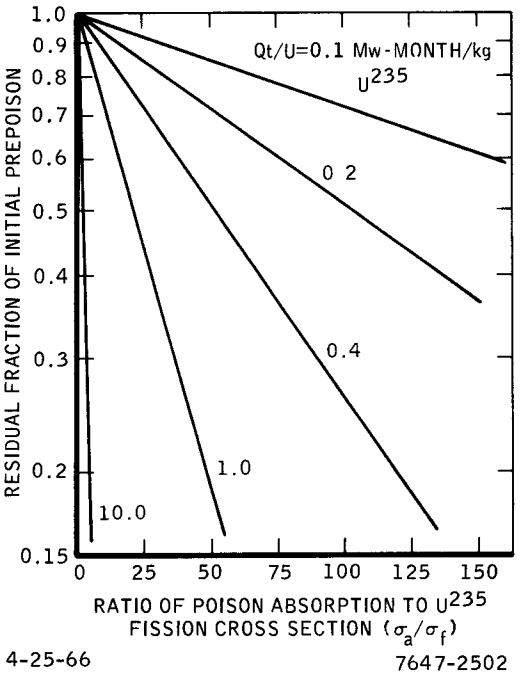

Figure 5. Fractional Residual Poison vs Poison Cross Section for Various Specific Energy Releases

TABLE 4

APPLICABILITY OF PREPOISONS FOR STATIC CONTROL

Poison	σ_a/σ_f, U^{235}	Optimum Qt/U for Static Control, $\frac{\text{Mw months}}{\text{kg } U^{235}}$
Gadolinium-157	160	<0.25
Samarium-149	110	0.25- 0.35
Cadmium-113	62	0.4 - 0.5
Gadolinium-155	44	0.5 - 0.8
Europium-151	16.4	4.0 - 6.0
Boron-10	6.3	8.0 -10.0

The above specific energy releases are approximate guidelines only. The optimum fraction of prepoison remaining at the end of life depends upon the temperature, power, and lifetime independently. Table 4 holds primarily for high-temperature (1300°F coolant outlet) reactors. As an example, the SNAP 10A reactor is fueled with 4.75 kg U^{235}. The appropriate power levels for each poison are then:

	Power Level (kw)		
	1 year	3 years	5 years
Gadolinium-157	<100	<35	<20
Samarium-149	100-140	35-45	20-30
Cadmium-113	160-200	50-70	30-40
Gadolinium-155	200-320	70-110	40-65
Europium-151	Power levels not practical for 10A type reactors		
Boron-10			

Gadolinium-157 is the poison exhibiting the highest effective cross section in a SNAP spectrum and therefore should be used for the lower power levels up to the limit indicated.

For a larger reactor having a U^{235} loading of 12 kg, appropriate power levels would be,

	Power Level (kw)		
	1 year	3 years	5 years
Gadolinium-157	<250	<85	<50
Samarium-149	250-350	85-120	50-70
Cadmium-113	400-500	130-170	80-100
Gadolinium-155	500-800	170-270	100-160
Europium-151	4,000-6,000	1,300-2,000	800-1,200
Boron-10	8,000-10,000	2,700-3,300	1,600-2,000

The formation of prepoison daughter products has not been considered in the above analysis. This omission is satisfactory for all poisons except europium-151.

If no poison exists which closely fits the desired application, poison mixtures should be used. The most common need for mixtures is for a gadolinium-155 - boron-10 mixture for power levels located between the levels of applicability for the two isotopes.

IV. NOMINAL TEMPERATURE PROFILES

A. CALCULATIONAL METHODS

The temperature-time profile of a SNAP reactor under static control depends upon the reactivity-time profile and the magnitude of the effective negative temperature coefficient. The calculation is made difficult, however, due to the fact that both the reactivity-time profile and the effective temperature profile depend in turn upon the temperature-time profile. These dependencies, which make an analytic solution of the reactor temperature impossible, are discussed below.

The strong dependence of reactivity profile on temperature profile is due primarily to the temperature-dependence of the hydrogen leakage reactivity loss. Hydrogen leakage, which is the major mode of operational reactivity loss at elevated temperatures, approximately doubles with every 50°F increase in temperature. Because of the mutual interdependence of reactivity loss and temperature profile shape, a stepwise calculation in time must be performed to determine the temperature profile. A digital computer program, LOAFER, has been written to perform these stepwise calculations. All modes of reactivity loss are considered. This code is described in the Appendix.

The effective temperature coefficient is itself dependent upon the reactor temperature. In addition to the variation in isothermal temperature coefficient with temperature, there exists a power-dependent addition to the coefficient. This contribution arises both from the normal power coefficient discussed in Section II and from the significant power-dependent xenon reactivity defect.

Since changes in xenon concentration lag power changes by only a few days, the concentration may always be assumed to be in equilibrium with the current power level for purposes of long-term temperature drift calculations. Since the power drift is related to temperature drift, this reactivity change can be expressed as part of the effective temperature coefficient,

$$\alpha_{eff,i} = \alpha_{iso,i} + \left(\frac{dP}{dT}\right)_i \alpha_{P,eff}$$

where

$\alpha_{eff,i}$ = effective temperature coefficient over time interval i ($\cent/°F$)

$\alpha_{iso,i}$ = isothermal temperature coefficient evaluated at reactor temperature over time interval i

$\left(\frac{dP}{dT}\right)_i$ = rate of change of reactor thermal power with reactor coolant average temperature evaluated over time interval i, and

$\alpha_{P,eff}$ = effective power coefficient ($\cent$/kw).

A relation was assumed between power and temperature of the form,

$$\frac{P}{P_o} = \left(\frac{T}{T_o}\right)^n$$

where the subscripts o refer to initial conditions and the temperature is the average coolant temperature in the core. For thermoelectric power conversion systems, the exponent n would be very close to 4.0 if the radiator temperature were the same as the core temperature, since the heat rejection follows the T^4 radiation law and because almost all of the heat produced in the reactor is rejected to space from the radiator. Since there are temperature drops between the core and the radiator, however, n is generally less than 4.0. Because of the large temperature drop across the thermoelectric elements, it has been found that n is approximately equal to 2.3 for temperatures in the range of interest for SNAP reactors. (The value of n is normally determined for a narrow range of operation for specific applications.) In this case,

$$\left(\frac{dP}{dT}\right)_i = 2.3\,\frac{P_o T_i^{1.3}}{T_o^{2.3}} = 2.3\,\frac{P_i}{T_i} \quad .$$

Also,

$$\alpha_{P,eff} = \alpha_P + \alpha_{xe}$$

where

α_P = power coefficient (¢/kw), and

α_{xe} = xenon coefficient (¢/kw).

The effective temperature coefficient is therefore given by,

$$\alpha_{eff,i} = \alpha_{iso,i} + 2.3 \frac{P_i}{T_i}(\alpha_P + \alpha_{xe}) \quad .$$

For a SNAP 10A type reactor,

$\alpha_P \approx -0.2¢/kw$

$\alpha_{xe} \approx -0.4¢/kw$, and

$\alpha_{iso} \approx -0.3¢/°F$;

or

$$\alpha_{eff,i} = -0.3 - 1.38 \frac{P_i}{T_i} .$$

For the SNAP 10A flight reactor,

$P_i \approx 40$ kw, and

$T_i \approx 950°F = 1410°R$;

or

$$\alpha_{eff} \approx -0.3 - 1.38 \frac{40}{1410} = -0.33¢/°F.$$

The power-dependent term under these conditions accounts for less than 10% of the total effective coefficient. At advanced performance conditions, however (250 kw at 1100°F core average temperature), the power-dependent terms become much more significant.

$$\alpha_{eff} = -0.3 - 1.38 \frac{250}{1560} = -0.3 - 0.22 = -0.52¢/°F \quad .$$

The power dependent terms are added to the isothermal temperature coefficient at each time step in the LOAFER code. The effect of these power dependent terms is to reduce the increase in temperature drift as the power is increased.

The magnitude of the negative temperature coefficient may be reduced somewhat by the addition of the prepoison. Since the cross section of most poisons decreases more rapidly than the $1/v$ dependence of the U^{235} fission cross section, the negative worth of the poison decreases as the neutron spectrum is hardened by the increase in temperature. This effect can be very significant for a poison with a cross section which exhibits a maximum in the vicinity of the peak of the neutron spectrum. Samarium-149 and other poisons in a SNAP spectrum exhibit this behavior (see Appendix C). Preliminary estimates indicate that the worth of samarium-149 may decrease as much as 10% as the temperature is raised from ambient to operating levels. For a heavy (~$6.00) loading, the worth will therefore decrease by about 60¢ over a temperature range of about 1000°F. If this effect is linear with temperature, a positive contribution to the temperature coefficient of about 0.06¢/°F arises. If the effect is not linear with temperature, it is quite possible that the presence of the poison can significantly decrease the magnitude of the negative temperature coefficient at operating temperatures.

B. SELECTION OF TEMPERATURE-TIME PROFILE

The selection of the temperature-time profile for a given application is essentially one of trial and error. The specification for a particular application will usually require a specific value for the minimum electric power output which must be supplied during the entire operating lifetime of the system. Since the efficiency of the power conversion system will degrade during operation, this requirement translates to one of specifying the minimum end-of-life temperature which can be tolerated. Evaluation of a nominal temperature drift therefore reduces to the following considerations:

1) Magnitude of the reactor temperature (generally specified as the coolant outlet temperature) at the end of the reactor operating life (EOL).

2) Minimum value of the reactor temperature at any time during life.

3) Maximum value of the reactor temperature at any time during life.

4) Magnitude of the reactivity penalty associated with the prepoison required to provide the temperature profile.

The following discussion deals primarily with higher temperature reactors (1200 to 1300°F) in which the hydrogen redistribution is completed during the first few days of operation. Possible types of temperature profiles for such reactors are shown in Figure 6. The three profiles assume the same required value for the EOL temperature.

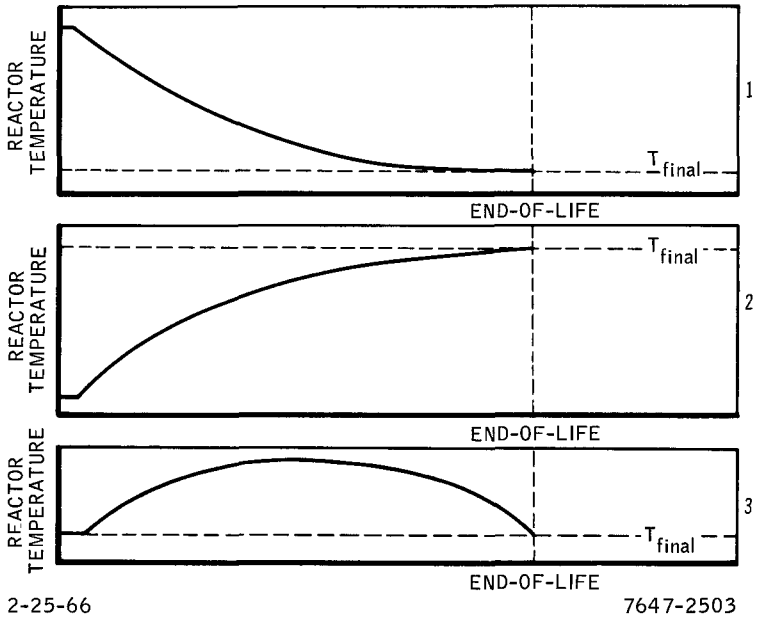

Figure 6. Possible Types of Temperature Profiles

Profile 1 demonstrates the situation in which the reactor is brought to an initial temperature higher than the required EOL temperature during the active control period. Following the termination of active control the reactor temperature steadily decreases to its final EOL value.

Profile 2 demonstrates the situation where the reactor temperature steadily increases during lifetime. The temperature during the active control period is maintained at a level below the EOL value.

Profile 3 is one in which the nominal initial temperature is chosen equal to the EOL temperature. The reactor temperature increases during the first half to two-thirds of the operating lifetime, following which time it falls to the nominal EOL value.

Profiles of type 1 will in general require the smallest amount of prepoisoning since sufficient poison is not required to balance the reactivity losses. However most power conversion system requirements specify temperature peaking of not greater than ~50°F. Since the effective temperature coefficient is about -0.5¢/°F, the reactivity must be balanced to within 25¢ during lifetime. The poison savings are therefore not significant. In addition, this type of profile can lead to excessively low temperatures should the reactivity losses be greater than predicted. The nature of the uncertainties in reactivity losses is considered in the next section.

Profiles of type 2 tend to provide a more nearly constant electrical output from the power conversion system since the heat source temperature is increasing to compensate partially for the degradation in efficiency of the power conversion system. The poison requirements are the largest for this profile since the reactivity input rate from prepoison burnout must always be greater than the reactivity loss rate. This effect is partially compensated by the fact that reactivity losses will be lower using this profile since the reactor temperature is always lower than for the other profiles. This profile is susceptible to the danger of excessively high temperatures, however, should reactivity losses be less than expected.

Profiles of type 3 have been selected as one of the many possible compromises. The prepoison concentrations required are greater than in case 1 but less than in case 2. Nominal temperature drifts during life are less severe, thereby minimizing the consequences of either upside or downside uncertainties in magnitudes of reactivity losses.

Having selected the type 3 profile, the problem reduces to finding the prepoison to provide the desired profile shape. The general considerations involved have been discussed in Section III. If more than one prepoison exists with cross sections in the range of interest, the isotope or mixture used should be selected as a compromise between excessive temperature peaking and higher initial loadings. Suppose, for example, that an application exists for which a mixture of samarium-149 and gadolinium-155 might serve as poison. There are an infinite number of potential mixtures of these poisons which will provide the desired EOL temperature. As the proportion of samarium-149 in the

mixture is increased, the total initial reactivity worth of the required prepoison mixture will decrease since a larger fraction of the mixture will be burning out during operating lifetime. Simultaneously, however, the increased fraction of the higher cross-section poison will cause more rapid initial poison burnout and therefore will cause more severe reactor temperature peaking during early periods of reactor life. Conversely, increasing the proportion of gadolinium-155 will increase the initial reactivity worth of the prepoison mixture but will reduce temperature peaking during life. The poison mixture selected should be that in which the nominal peaking is at the maximum acceptable level.

This process is of necessity trial-and-error because of the strong dependence of the hydrogen leakage on the temperature profile.

For low temperature operation (~1100 to 1150°F coolant outlet temperatures), the hydrogen redistribution will not be completed during the active control period. At some temperatures continuation of redistribution after the active control period may cause reactivity losses too rapid to be conveniently compensated by a prepoison. In this case the temperature profile may show an initial large temperature drop prior to completion of the redistribution.

This effect may be eliminated by operating for a short period at a temperature sufficiently high to allow the rapid completion of hydrogen redistribution. Another method would be to raise the temperature sufficiently to compensate for the reactivity loss associated with hydrogen redistribution by the reactivity gained as the temperature falls, such that the temperature reaches the desired starting point when hydrogen redistribution is complete. Calculational procedures are similar for any of the approaches mentioned.

V. UNCERTAINTIES IN REACTOR PERFORMANCE

The preceding sections deal with the prediction of the nominal behavior of reactors under static control. Because of the lack of external reactor control during this period, however, any departure of the reactivity losses from their nominal value will result in a deviation in reactor temperature from its predicted value. Since the performance of the power conversion system depends to a large degree on the heat source temperature, the potential variations in reactor temperature due to these uncertainties can seriously compromise the system success if not properly compensated. The major contributors to uncertainty in the reactor EOL temperature are uncertainties in hydrogen leakage rate, prepoison burnout rate, reactivity depletion rate due to fission effects (fuel depletion and fission product accumulation), and initial reactor temperature set point. In addition, uncertainties in the magnitude and time constant of hydrogen redistribution contribute to the EOL temperature uncertainty for low temperature reactors in which a significant amount of redistribution remains to be completed during the static control period. These major contributore are discussed below.

A. HYDROGEN LEAKAGE RATE UNCERTAINTY

Hydrogen leakage rate is a function of the internal hydrogen pressure, the temperature distribution along the hydrogen barrier, and the type and condition of the barrier. The hydrogen pressure depends upon the temperature distribution in the fuel and the hydrogen concentration distribution in the fuel. The temperature distribution in the fuel in turn depends upon the thermal conductivities of fuel and cladding materials and the power being generated in the particular rod. The temperature distribution along the hydrogen barrier depends on the axial power distribution along the fuel rod and the coolant flow distribution. Changes in any of these quantities during operation of the reactor will result in change in hydrogen leakage rate. Most probable causes of changes in leak rate during operation are physical damage or degradation of the hydrogen barrier during operation or decrease in fuel thermal conductivities due to hydrogen depletion.

B. PREPOISON BURNOUT RATE UNCERTAINTY

Uncertainties in prepoison burnout rate arise both from uncertainties in poison loading and uncertainties in poison microscopic poison cross section in a SNAP operating neutron spectrum. The worth of the poison loading at ambient temperature is generally obtained by measuring the difference in reactivity in a critical assembly before and after the application of the hydrogen barrier containing the prepoison. Errors arise both because of the long period of time between these measurements and the inherent uncertainty in a differential reactivity measurement.

Even if the concentration of the prepoison and its reactivity worth at ambient temperatures can be measured, errors are introduced by the change in prepoison worth (and therefore burnout rate) as the temperature is increased to operating levels. This phenomenon is primarily due to the difference between the energy-dependence of the fuel and prepoison cross sections. This effect is particularly significant in the use of samarium-149, whose cross section exhibits a resonance in the vicinity of the peak in the zirconium-hydride-moderated neutron spectrum.

C. UNCERTAINTY IN FISSION REACTIVITY EFFECTS

Both the depletion of fuel and the buildup of fission products contribute to reactivity losses during reactor operation. These losses, which are the primary losses during low-temperature operation, become less significant as hydrogen leakage increases with increasing temperature. Because of the small burnups in SNAP reactors, these reactivity losses are essentially linear with energy release. Incremental worths of U^{235} have been measured in the SCA-4 critical assembly.[5] Reactivity losses due to buildup of fission products have been calculated by the use of the SIZZLE burnup code[6] using the cross sections as described in Section II. The SIZZLE code performs a series of one-dimensional diffusion theory calculations stepwise in time. Burnup calculations are performed at each time step using a six-energy group reduction of the sixteen-group energy structure. The worth of fission products was determined by running the SIZZLE code twice for the desired operating period. For the initial run the fission product cross sections were inserted; a second run was

made with the fission product cross sections set equal to zero. The difference in reactivity loss between these two runs was taken as the reactivity loss introduced by fission product accumulation. Infinite-cylindrical geometry (radial dependence only) was used in the calculations; the effects of axial dependence were estimated by synthesis technique.

These reactivity worths have not yet been satisfactorily measured in an operating SNAP reactor. Reliance on calculations, in the case of fission product worth, and measurements at ambient temperatures, in the case of fuel depletion, introduce uncertainties in the predictions of these operating reactivity losses.

D. INITIAL TEMPERATURE SET-POINT UNCERTAINTY

During the active control period the reactor temperature is maintained within a dead band by insertion of reactivity by the control system whenever the temperature drops below the lower end of the dead band. Reactivity is inserted until the upper end of the dead band is reached. The temperature during the active control period may therefore be considered random within the dead band during the active control period. If the active control period is terminated at a preset time, the temperature at the initiation of static control can be anywhere within the dead band width. Since reactivity losses are temperature-dependent, departure of the temperature at the beginning of static control from the nominal level will introduce an uncertainty in EOL temperature.

In addition to random positioning within the dead band, the entire band itself may be shifted upward or downward due to errors in presetting and tolerances in operation.

E. ASSUMED MAGNITUDE OF UNCERTAINTIES

The following magnitudes of uncertainties for each reactivity effect have been assumed for the purpose of uncertainty analysis.

1) Hydrogen Leakage. Because of the difficulty in predicting probable uncertainty limits on hydrogen leakage in future high-temperature reactors, the uncertainty in hydrogen leakage rate has been left as a variable.

2) Prepoison Burnout Rate. The sum of spectral effects and loading uncertainties has been taken as equal to 10% of the nominal poison loading.

3) Fission Effects Uncertainties. An uncertainty of 20% in the reactivity worth of fuel depletion and fission product accumulation has been assumed.

4) Temperature Set Point. An uncertainty in the reactor temperature of ±20°F at the initiation of static control has been assumed.

F. CALCULATION OF EOL TEMPERATURE UNCERTAINTIES

Uncertainty quotations were initially made on a "worst possible case" basis. Individual contributions to uncertainty were determined on the integral basis described below and were summed to provide the maximum temperature uncertainty. These individual contributions were approximated by multiplying the nominal reactivity loss due to the effect by an assumed fractional uncertainty to obtain the reactivity uncertainty due to that effect. This reactivity uncertainty was then divided by an effective temperature coefficient to provide the individual contribution to the temperature uncertainty. For example, at a power of 250 kwt for 1 yr, the fission product and fuel depletion reactivity loss is approximately 75¢. If an uncertainty of 10% is assumed in this calculation, the reactivity uncertainty is ±7.5¢. This was translated into a temperature uncertainty of ±15°F using an effective temperature coefficient, modified to include system feedback effects, of -0.5¢/°F. This uncertainty was added to uncertainties due to other effects.

This approach is valid only for the improbable case of all reactivity effects simultaneously being at their maximum value in the same direction. Uncertainty calculations were therefore modified to calculate the total uncertainty on a more reasonable basis. The individual uncertainties were calculated assuming that the uncertainty was in the direction that would result in greater than nominal reactivity loss. These individual uncertainties were combined by taking the root-mean-square of their sum. This method, while not rigorous, was considered a more reasonable approach to the determination of the temperature uncertainty. The effects are not independent and therefore the root-mean-square is not directly applicable. Also, the direct addition of all the uncertainties is unreasonable, since hydrogen leakage exhibits a strong feedback effect

as the temperature changes. The root-mean-square of the sum of the individual uncertainties is used to define the total end-of-life temperature uncertainties shown in Figures 7, 8, and 9.

Use of the LOAFER code makes it possible to include the "hydrogen leakage feedback" in calculations of individual uncertainty effects. This calculation is more accurate than the integral method described above. The leakage feedback effect, arising due to the strong influence of temperature on hydrogen leak rate, is discussed below. Individual contributions to the end-of-life uncertainty are calculated in this manner and the root-mean-square is taken as the composite EOL temperature uncertainty.

G. HYDROGEN LEAKAGE FEEDBACK

"Hydrogen leakage feedback" is the term applied to that phenomenon by which the changes in hydrogen leakage with changes in temperature tend to reduce the temperature drift causing the change in hydrogen leakage. This feedback tends to considerably damp those temperature uncertainties which might otherwise arise. If, for example, some reactivity effect is greater, i.e., more negative, than predicted, the reactor temperature will tend to drift lower than predicted. The lower temperatures, however, will lead to lower-than-predicted hydrogen leakage because of the strong temperature dependence of leakage. This lower leakage will tend to retard the downward temperature drift. Should the loss be less than expected, the reverse argument holds true. Hydrogen leakage in a sense can therefore be thought of as an irreversible negative temperature coefficient.

Hydrogen leakage can also feed back upon itself. An illustration of this effect is shown in Figure 10. This figure shows the factor by which the leakage throughout the reactor design life (integrated leakage) is increased by errors in predicted initial leak rate.

The effects of hydrogen depletion are illustrated in the Active Control curve. In this case it is assumed that the control system holds the temperature constant. It is seen that the integrated leakage does not increase linearly with initial leak rate due to the drop in hydrogen pressure driving force accompanying hydrogen depletion. For example, should the initial leak rate be three times nominal, the integrated leakage is increased by only a factor of 2.27.

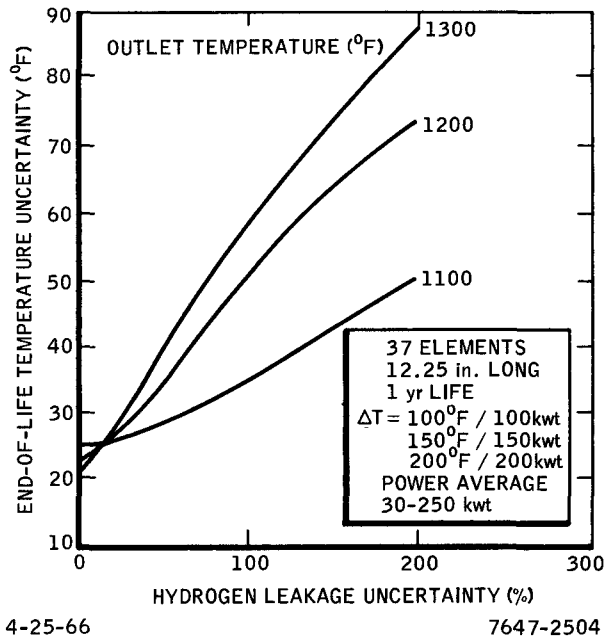

Figure 7. Averaged Temperature Uncertainty vs Hydrogen Leakage Uncertainty, 1-yr Life

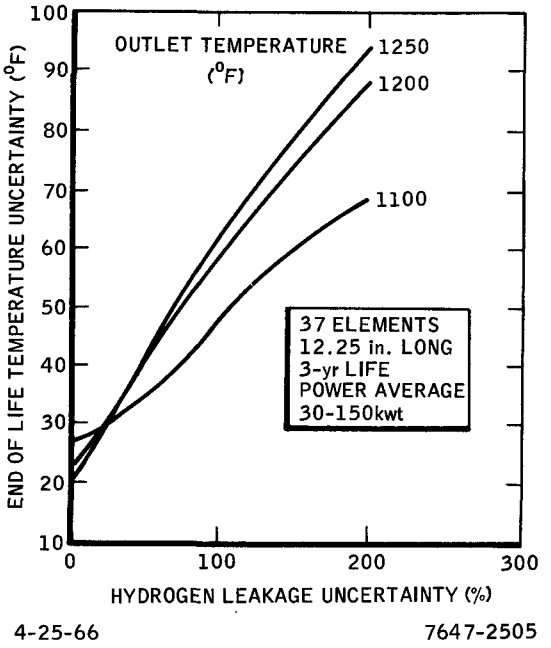

Figure 8. Averaged Temperature Uncertainty vs Hydrogen Leakage Uncertainty, 3-yr Life

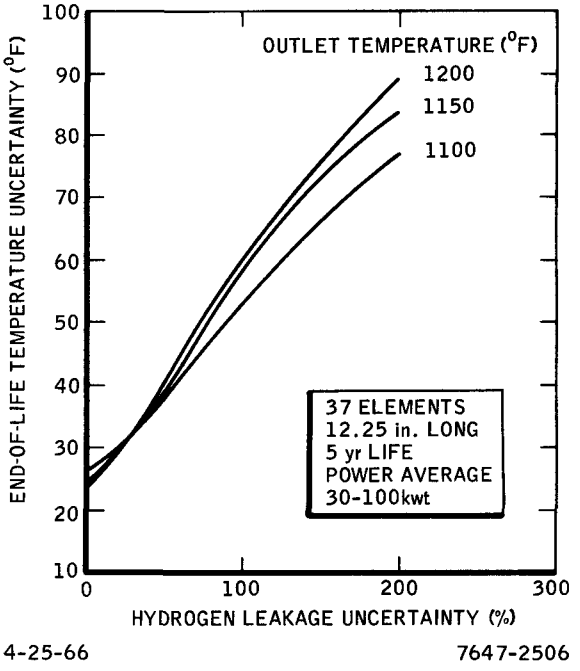

Figure 9. Averaged Temperature Uncertainty vs Hydrogen Leakage Uncertainty, 5-yr Life

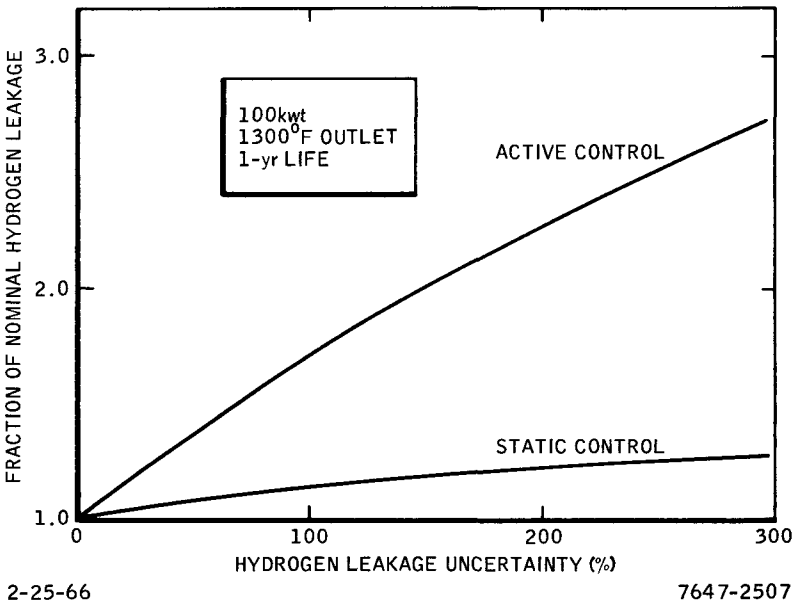

Figure 10. Examples of Hydrogen Leakage Feedback Effects

The most powerful effect, however, is that due to the temperature dependency of leak rate. The Static Control curve allows the temperature to drop to compensate for the increased leakage. The drop in temperature causes a decrease in integrated leakage below what would be obtained were the temperature held constant, as in active control. In the case quoted above of an initial leak rate three times nominal, for example, the integrated leakage would increase by a factor of only 1.22. The accompanying temperature decrease would be only 70°F whereas hundreds of degrees drift would be present should neither effect exist.

As an example of the effects of leakage feedback, results of a short uncertainty study performed on the SNAP 10B (Figure 7) reactor model are presented.[7] Figures 7-9 show the temperature uncertainties under static control for 1, 3, and 5 years of operation for coolant outlet temperatures of 1100, 1200, and 1300°F. Reactor power is not shown as a parameter since EOL temperature was found not to be a significant function of reactor power.

At first glance some of the results appear to be contrary to intuitive opinion. Fuller explanations of two of the apparent anomolies are presented below.

1) The apparent decreasing effect of outlet temperature on end-of-life uncertainty at elevated temperatures, i.e., the decreasing rate of increase of temperature uncertainty with temperature at higher temperature levels. Figure 7 yields the following temperature uncertainties for 1 yr of operation at 100% hydrogen leakage rate uncertainty.

Outlet Temperature (°F)	End-of-Life Temperature Uncertainty (°F)
1100	35
1200	50
1300	59

It is seen that the increase in uncertainty from 1100 to 1200°F outlet temperature is larger than the increase in uncertainty from 1200 to 1300°F. Since the hydrogen leakage rate is strongly dependent on temperature, this result seems contrary to intuition.

2) The relative independence of temperature uncertainties of operating lifetime. Figures 8 and 9 can almost be superimposed for the higher-temperature (1200 and 1300°F outlet) cases while the results for the 1100°F outlet cases show slight increases in uncertainties with lifetime. Since hydrogen leakage increases with lifetime, this result appears to be unreasonable.

Both of these effects, however, are real and are explained in more detail below.

H. DEFINITION OF TERMS

An important distinction is that between hydrogen leakage rate uncertainty and integrated hydrogen leakage uncertainty. The "cause" here is uncertainty in hydrogen leakage rate. This uncertainty is due to inability to calculate leakage rates as function of power and temperature — given permeation data from a particular isothermal temperature test — and to possible degradation of the hydrogen barrier during reactor operation. Over a small temperature interval it is convenient to express this uncertainty as a percent of nominal leakage rate. For example, a set of elements with a 50% leakage uncertainty is assumed to have a leak rate between 0.5 and 1.5 of the nominal calculated leak

rate. This definition is imperfect in that errors in calculation will not in general be expressible as constant fractions of the calculated rate, so that the uncertainty multiplier changes with temperature. The uncertainty factor chosen for analysis, therefore, should be appropriate to the particular temperature level being considered. Alternately, for survey calculations, a single factor may be chosen which is large enough to be suitable for all temperatures under investigation.

As mentioned above, though the uncertainty in leak rate is the cause, the effect is uncertainty in integrated leakage. It is this latter quantity that is of direct importance in static-control reactor analysis since it is the integrated leakage uncertainty which determines that portion of the temperature uncertainty which is due to hydrogen leakage uncertainty. In general, the uncertainty in resultant integrated leakage is much smaller than the uncertainty in the instantaneous leakage rate. This effect is due both to the reduction in leakage rate accompanying hydrogen depletion and the reduction in leakage rate provided by lower temperature operation. This hydrogen leakage feedback effect was described previously.

I. EFFECT OF TEMPERATURE LEVEL ON TEMPERATURE UNCERTAINTIES

An increase in the reactor temperature level changes the integrated hydrogen leakage uncertainty, and therefore the end-of-life temperature uncertainty, in two ways at a given leakage rate uncertainty. First, the magnitude of the nominal leakage increases with temperature, doubling with every 50°F increase in temperature. The effect of hydrogen leakage feedback, however, strongly increases with temperature. This effect is shown in Figure 11 where the integrated leakage, normalized to the nominal leakage, is shown as a function of leakage rate uncertainty, expressed as actual leakage rate divided by predicted leakage rate. It is seen that hydrogen leakage feedback is rather small at 1100°F, while it is extremely large at 1400°F. At the limit of very high temperatures, the curve would be a horizontal line at 1.0 since all hydrogen would leak out and an increase in uncertainty could cause no further leakage increase.

The absolute increase in integrated hydrogen leakage with leakage rate uncertainty is a combination of the two opposing effects. The increase in nominal

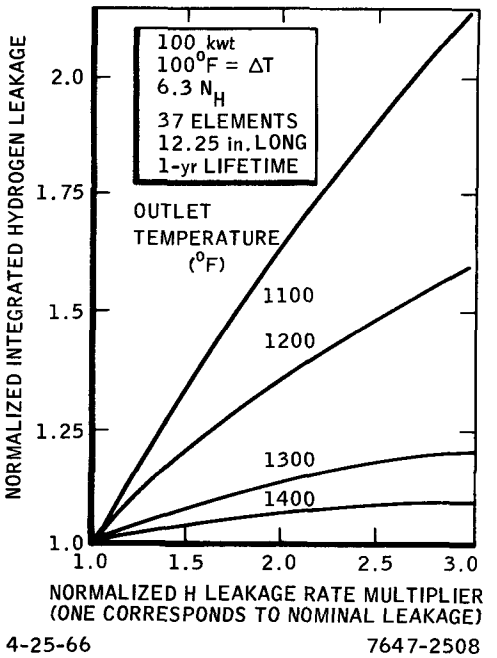

Figure 11. Normalized Hydrogen Leakage as a Function of Leakage Multiplier

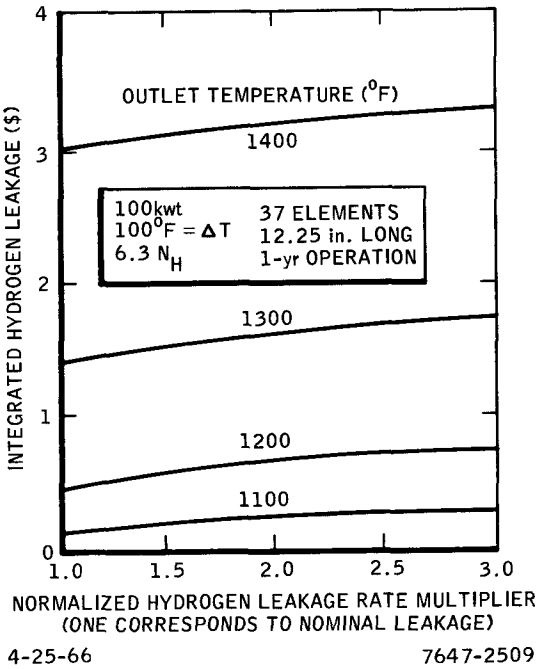

Figure 12. Absolute Integrated Hydrogen Leakage as a Function of Leakage Multiplier

hydrogen leakage with temperature tends to cause increased uncertainties in integrated leakage with temperature at a given leakage rate uncertainty. The increased feedback with temperature, however, tends to reduce the increase in integrated leakage with temperature at a given leakage rate uncertainty. The result of these opposing factors is shown in Figure 12. The increase in absolute integrated leakage is shown as a function of leakage rate multiplier (a value of 1.0 corresponds to nominal rate, a value of 2.0 to twice the nominal rate, etc.). It is seen that the increase in integrated leakage, above nominal leakage, does not greatly increase with temperature even though the nominal leakage sharply increases with temperature. At a given leakage rate uncertainty, therefore, the integrated leakage uncertainty does not markedly increase with temperature.

J. EFFECT OF LIFETIME ON TEMPERATURE UNCERTAINTIES

The arguments here are similar to those of the preceding section. Nominal leakage shows a sharp increase with lifetime, as shown in Figure 13.* On the other hand, the effects of hydrogen leakage feedback also increase markedly with lifetime, as shown in Figure 14. Two opposing effects, increased nominal leakage vs increased feedback, therefore, are present as lifetime is increased. The resultant leakage changes are shown in Figure 15. It is seen that, although leakage does increase with lifetime, the change in absolute integrated leakage with lifetime at a given rate uncertainty factor is not large.

K. SECONDARY CONTRIBUTIONS TO EOL TEMPERATURE UNCERTAINTIES

Many secondary effects make minor contributions towards EOL temperature uncertainties. These effects are discussed by example below.

1) Core ΔT. A departure from nominal ΔT changes hydrogen leakage reactivity losses due to changes in fuel and cladding temperature profiles.

2) Heat Transfer Coefficients. Changes in heat transfer coefficients change hydrogen leakage through changes in fuel and cladding temperatures.

3) Fuel Rod Size. Small tolerances in fuel slug diameter change hydrogen leakage by changes in radial temperature distributions in the fuel rod.

4) Cladding Tube Diameter. Increases in cladding tube diameter increase the fuel-cladding gap causing increased fuel temperatures and increased hydrogen leakage.

5) Fuel Element Carbon Content. An increase in carbon content increases the effective H/Zr ratio and therefore the hydrogen leakage.

*The figure shown also has a positive second derivative. It would be expected to show a negative second derivative due to the falling off of internal hydrogen pressure with hydrogen depletion. The explanation of this behavior lies in the shape of the temperature-time profiles. Although the outlet temperature starts at 1350°F and falls to 1300°F at the end-of-life for all lifetimes, the differing amounts of poisoning cause different profile shapes. The large amount of poison required for long lifetimes causes some temperature peaking at beginning of life. The time-averaged temperature is therefore higher for longer-lived cases. This phenomenon does not affect the arguments presented.

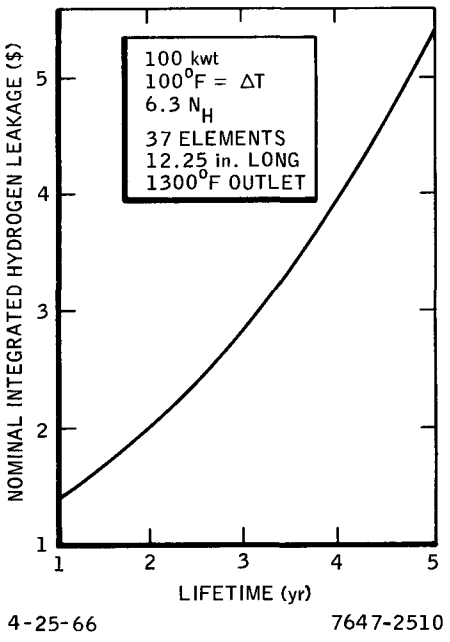

Figure 13. Integrated Hydrogen Leakage vs Lifetime

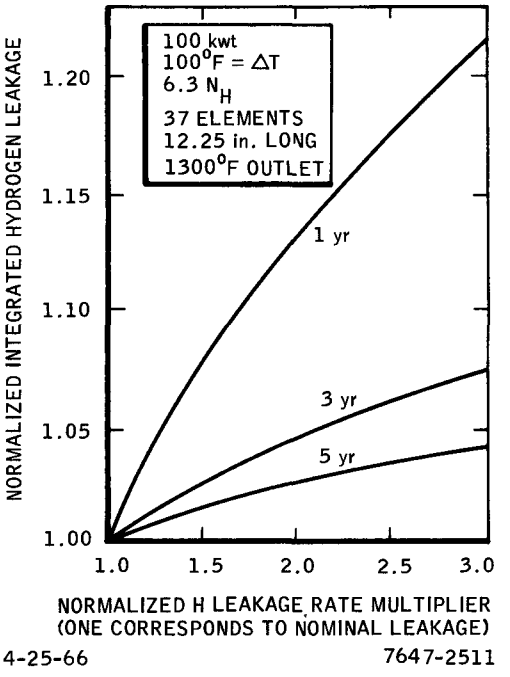

Figure 14. Normalized Leakage as a Function of Leakage Multiplier

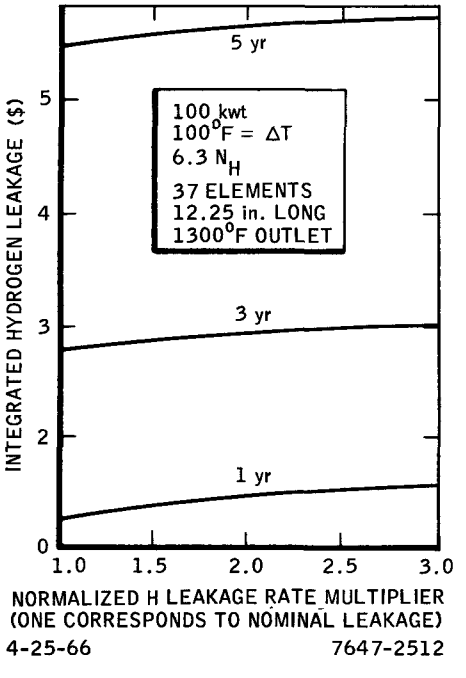

Figure 15. Absolute Integrated Hydrogen Leakage as a Function of Leakage Multiplier

6) Hydrogen Worth Calculations. Previous calculations of the reactivity consequences of hydrogen leakage have used experimental hydrogen worth profiles normalized to a volume-averaged worth of \$1.00/0.1 N_H unit. This value has been measured in the SCA-4A critical assembly and has been closely matched by analytical techniques. Should the actual hydrogen worth differ from the predicted value, additional end-of-life temperature uncertainty would result.

7) Fuel Alloy Uranium Content. Increase in fuel alloy uranium content increases the effective H/Zr ratio, thereby increasing hydrogen leakage and end-of-life temperature uncertainty.

8) Uranium-235 Loading. Increases in the U^{235} loading decreases the flux level for a given thermal power output. Burnout of prepoison is therefore slower than expected.

9) Reactor Power-Temperature Relationship. During static control reactor temperature and power are related by the equation,

$$\frac{P}{P_o} = \left(\frac{T}{T_o}\right)^n$$

where P_o and T_o are the initial thermal power and core average absolute temperature. From a study of thermoelectric converter systems it has been determined that n is approximately equal to 2.3. For Mercury-Rankine systems n is about 0.2. Should the reactivity change during static control, the power and temperature simultaneously move to new equilibrium values. The power change, through the power reactivity coefficient, makes a contribution toward the effective temperature coefficient. Uncertainties in the exponent therefore lead to uncertainties in the effective temperature coefficient and increased end-of-life temperature uncertainty.

10) Temperature Coefficient. The effects of uncertainties in isothermal temperature coefficients have been determined.

11) Samarium Cross Section. Effects of errors in the ratio of samarium absorption to uranium fission cross section have been included in this study.

This effect, caused by a change in the ratio of cross sections with temperature is different from that of errors in the loading, which was previously considered.

12) Hydrogen Concentration. Errors in predictions in hydrogen leakage due to errors in hydrogen concentration rather than barrier properties have been taken into account.

The effects of these uncertainties have been investigated for SNAP reactors and some results are shown in Figures 7-9. The results are detailed in Table 5. Using a root-mean-square method for summing uncertainties, these effects do not significantly increase EOL temperature uncertainty.

TABLE 5

SECONDARY CONTRIBUTIONS TO EOL TEMPERATURE UNCERTAINTIES

Effect	Assumed Uncertainty	Resultant Contribution to EOL Temperature Uncertainty (°F)
Core ΔT (°F)	20	0.5
Heat Transfer Coefficients (%)	25	9
Fuel Slug Diameter (mil)	10	1.5
Fuel-Cladding Gap Size (%)	20	3
Carbon Concentration (wt %)	0.05 (absolute)	6
Uranium Concentration (wt %)	0.5 (absolute)	7
Hydrogen Worth (%)	10	9
Uranium-235 Loading (kg)	0.15	1.5
Exponent on Power-Temperature Relationship (%)	20	1
Isothermal Temperature Coefficient (¢/°F)	0.05	2
Hydrogen Concentration N_H Units	0.03	6

VI. SNAP STATIC CONTROL EXPERIMENTS

Two SNAP 10A reactors have been operated using the static control mode. Their performance will now be discussed in more detail. In arriving at the evaluation of the performance of these two reactors, the performances of the preceding experimental SNAP reactors – SER, SDR, and S8ER – were considered.

The SNAP 10A performance predictions were based on calculated values for each of the reactivity effects. It was calculated that xenon would be 95% saturated after 32 hr of full power operation and would be compensated by control drum movement during the active control period. It was estimated that hydrogen redistribution would be essentially complete within 3 weeks with approximately 50% of the redistribution complete and compensated for by control drum movement during the first 72 hr. It was calculated that, after the first 3 weeks, fission product accumulation and fuel burnup would be the major reactivity loss mechanisms. Because of the relatively low operating temperature, hydrogen leakage was expected to cause only about one-fifth of the reactivity loss caused by fission product accumulation and burnup.

After making the above determinations, the samarium required in excess of equilibrium was determined so that its burnout would completely compensate for all reactivity losses after the completion of hydrogen redistribution. The reactor cores were fabricated with the appropriate amount of samarium oxide, and the predictions shown in Figure 16 were made. The minimum and maximum predicted lines were established after the assignment of uncertainty values to each of the reactivity loss mechanisms. As Figure 16 shows, it was expected that continuing hydrogen redistribution would cause the average temperature to fall for approximately the first 3 weeks and then, as redistribution was completed, the average temperature would slowly increase for the remainder of the 1-yr design life.

After receipt of the single startup command, the reactor was brought to operating conditions and stabilized by the automatic control system. The control system was deactivated after 72 hr. This marked the start of the static control period. Based on the temperature at that time, the predicted year-end temperature was 944^{+42}_{-39}°F.

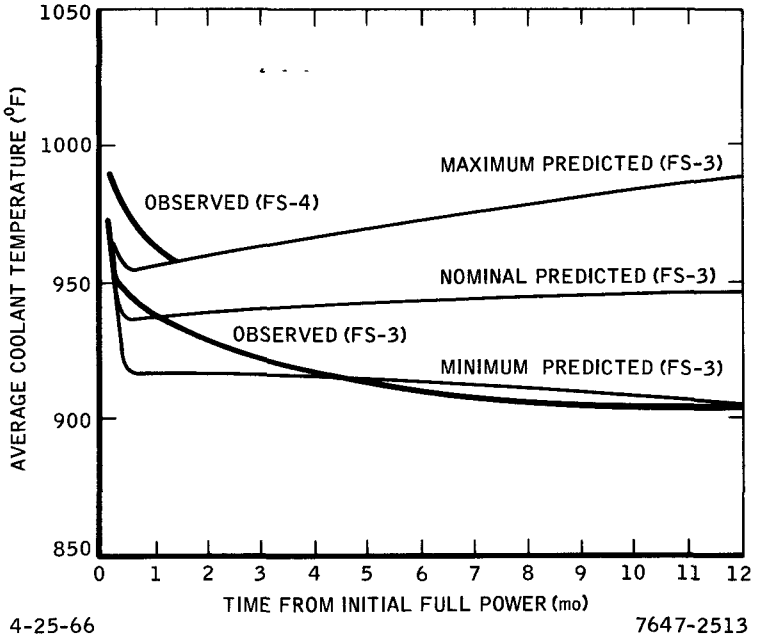

Figure 16. SNAP 10A Predicted and Observed Temperature Drift

On March 15, 1966, 10FS-3 was shut down after operating without interruption for 10,000 hr. This is the longest continuous run at design power for any known reactor. The average temperature in the reactor has continued to decrease slowly as shown in Figure 16. The average temperature was approximately 906°F at the end of 1 yr, slightly above the minimum predicted year-end temperature.

On April 3, 1965 the SNAP 10A flight test reactor (FS-4) was launched into polar orbit from Vandenberg Air Force Base. It, too, was started by a single startup command. The reactor was brought to power normally by the automatic control system and was automatically stabilized during the period of initial reactivity transients. Because of the temperature drift experienced on FS-3, the control system was allowed to operate for 6 days. At the end of this time, a ground command was given to raise the temperature slightly and then the control system was deactivated. The temperature is shown as a function of time following this in Figure 17. The FS-3 temperature behavior is also shown for comparison. The higher operating temperature of FS-4 was established to allow for the expected temperature drift based on FS-3 experience. Of particular significance is the similarity in drift rate between the two reactors. This

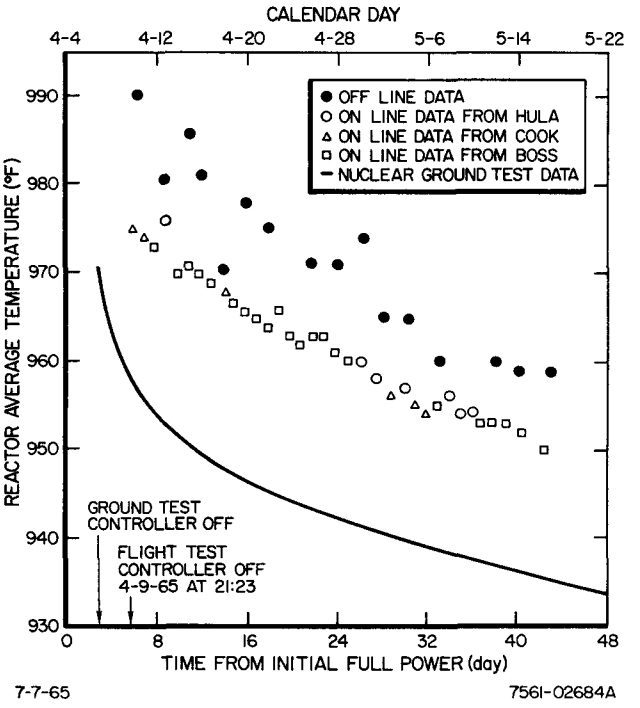

Figure 17. SNAP 10AFS-4
Temperature Drift

indicates that no observable random reactivity effects were present and that flight test performance can be accurately determined by ground test. After 43 days in orbit, a failure in the satellite electrical system, not related to the reactor operation, occurred causing termination of the FS-4 test.

With the added experience obtained from S8ER, FS-3, and FS-4 reactor operation, the analytical model for the SNAP reactors has been reexamined. There appear to be two primary reasons for the difference in characteristic shapes of the predicted and observed temperature drift curves for the SNAP 10A reactors. In addition, a small difference on FS-3 can possibly be attributed to modifications made in the reflector mounting to allow remote disassembly. These modifications may have allowed slight movement of the reflector during the heating period.

The first primary reason for the performance difference is the larger-than-expected time constant for hydrogen redistribution. The only operating experience on hydrogen redistribution prior to FS-3 was with the SDR. There was considerable uncertainty in the interpretation of this data, so a computed time

constant was used in the predictions. This value, 90 hr, was determined using hydrogen diffusion coefficients available in the literature and a hydrogen redistribution analytical model. With the added data from S8ER, FS-3, and FS-4, the relationship between hydrogen redistribution time constant and temperature has been fairly well established. At an average coolant temperature of 950°F, corresponding to the early part of the static control period on FS-3, the time constant is about 1500 hr. As the temperature drops, the time constant increases to a value of 3000 hr at 900°F. The effect of the longer time constant is that more hydrogen redistribution takes place during the static control period and the redistribution is much more gradual, not being completed within the first month as originally predicted. The large difference between the experimentally determined time constant and the computed value resulted from an error in the analytical model used.

The other primary reason for a difference in temperature performance was the greater-than-expected reduction in samarium worth with increasing temperature. Early data showed approximately a 3% reduction in samarium worth in the zirconium hydride neutron spectrum when raising the temperature from ambient to 900°F. More recent data show this reduction is about 10%. Since SNAP 10A had to be prepoisoned to only about 40% above equilibrium samarium concentration, the 10% shift in the total samarium had a fairly significant effect on the differential worth above equilibrium. With this reduction the burnout of samarium was not sufficient to compensate for reactivity losses other than hydrogen redistribution, so that the temperature drift curve asymptote, which is approached as redistribution is completed, has a slight negative slope.

Figure 18 shows the effect on average reactor temperature of each of the reactivity loss mechanisms as they are now estimated. The total curve is an addition of all of the individual curves and is very close to the observed FS-3 temperature curve. Of significance is the fact that the FS-3 drift can be matched with near nominal values for all of the individual loss mechanisms.

The FS-3 and FS-4 experience has shown that static control is definitely feasible for reactors operating in the temperature and power range of SNAP 10A. Valuable information was obtained from this operation for use in analysis of more advanced static control reactors.

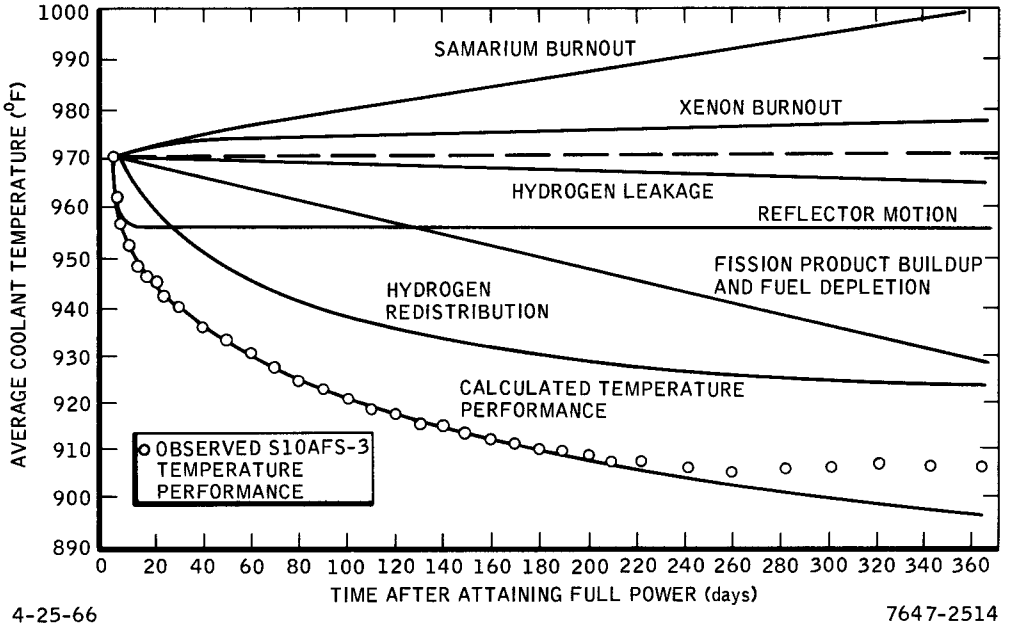

Figure 18. Effect of Individual Reactivity Loss Mechanisms on Average Reactor Temperature

VII. ADVANCED UTILIZATION OF STATIC CONTROL

It is possible to design SNAP reactors to operate on a nominal basis under static control for any design conditions for which active control operation is possible. Operation is limited, however, to the temperature range below 1300°F core outlet by the uncertainties in hydrogen leakage. If improved barrier materials are developed (i.e., barriers capable of retaining hydrogen at higher temperatures) the use of static control will become practical at higher temperatures.

The use of static control limits the reactor application since rapid changes in power requirements cannot be tolerated unless the unnecessary power can be dumped. That is, a statically-controlled reactor must operate at nearly constant power and cannot compensate for changes in load requirements.

A. NOMINAL OPERATION

A poison or combination of poisons can usually be found to assure that reactivity insertion due to prepoison burnout will approximate the operational reactivity loss profile. For long-lived, high temperature applications, this selection will be expensive, since a large amount of a low cross section material will have to be employed to avoid premature poison burnout. The size of a statically-controlled reactor will therefore tend to be larger than that of an actively-controlled reactor. The reflector on a SNAP 8 reactor designed for 1 Mwt operation for 1 yr at 1300°F will be approximately 2 in. thicker due to the necessity to compensate for the high prepoison loading. The weight penalty will increase as the lifetime is increased. It has been determined, however, that weight penalties do not seem to become excessive before some other operational limit (e.g., thermal or material limits) is reached.

B. UNCERTAINTIES IN OPERATION

Studies of EOL temperature uncertainties for reactors such as SNAP 8 indicate that these uncertainties are similar to those calculated for the SNAP 10B reactor. Since most power conversion systems require a temperature uncertainty limit in the vicinity of ±50°F for satisfactory operation, hydrogen leakage rates must be predictable to within about 100%. It should be reemphasized that

this figure represents uncertainties in leakage rate, not in integrated leakage. If temperatures or lifetimes are increased to a point where hydrogen leakage rate cannot be predicted within this band, static control will not be feasible.

C. STATIC CONTROL VERSUS ACTIVE CONTROL

The use of static control provides opportunities for generation of electric power with no moving parts. No dependence is placed on automatic control equipment for extended periods of time. Problems introduced by the requirement for motion, such as self-welding in the vacuum of space, are eliminated. These considerations tend to enhance the reliability of the power generation unit.

For high power, high temperature applications, however, the use of static control introduces several disadvantages. The reactor is heavier because of the need to compensate for the prepoison loading which will not completely burn out during life. Reasonably-accurate (within 100%) predictions of hydrogen leakage rates must be made to avoid excessive temperature uncertainties.

It appears, under the present state-of-the-art, that static control is most attractive for low temperature ($\leq$1200°F core outlet) remote applications. The ability of these reactors to operate with no moving parts for periods of several years should prove attractive for both space and undersea applications. At higher temperatures (>1300°F core outlet), however, hydrogen leakage cannot be predicted within the necessary band. Further improvements in this prediction are necessary before static control can be applied to higher temperature applications. For manned applications, where it will probably be desirable to shut down and restart the reactor, static control loses some of its attractiveness.

A potentially attractive design approach would be to design and prepoison the reactor for static control but to employ an active control system. This mode of operation could minimize the consequences of failure of the control system. The use of an active control system in conjunction with the static control design allows the system to be used for many more applications. Such a power source has the capability to follow the load requirements and is not limited to nearly constant power operation.

REFERENCES

1. D. F. Atkins, "Dissociation Pressures of Hydrided Zirconium - Uranium Alloys," NAA-SR-4245 (February 15, 1960)

2. J. Miller, et al., "Temperature Coefficients and Spectra in the Hydride Moderated SNAP Reactors," NAA-SR-7140 (December 30, 1962)

3. L. M. Fead, et al., "SNAP 8 Experimental Reactor Operations and Test Results," NAA-SR-10903 (June 28, 1965)

4. H. S. Isbin, "Introductory Nuclear Reactor Theory," Reinhold Publishing Corp. (New York, 1963)

5. D. W. Clifford, "Final Report on the SNAP 10A Prototype Critical Assembly Studies," NAA-SR-8613 (April 30, 1964)

6. D. P. Satkus and H. P. Flatt, "SIZZLE," NAA Program Description (February 1961)

7. R. J. Gimera, "SNAP 10B Reactor Conceptual Design," NAA-SR-MEMO-10422 (November 20, 1964)

APPENDIX

A. REACTIVITY CALCULATIONS

Temperature/time profiles were determined using the LOAFER digital computer code. This program performs a stepwise calculation of reactivity, temperature, and power. All modes of reactivity loss (hydrogen leakage, fission product accumulation, fuel depletion, xenon buildup, hydrogen redistribution, temperature and power defect, and prepoison burnout) are considered. Feedback from the system is simulated by a relationship between temperature and power degradation in the reactor. Hydrogen leakage rates are calculated at each time step and are therefore appropriate to the current reactor power, temperatures, and current depleted hydrogen level. Spatial temperature profiles across the reactor are generated so that spatial hydrogen leakage can be calculated.

In a simplified form, the code solves the following equations:

$$T_{i+1} = T_i + \frac{\Delta\rho_i}{\alpha_{eff,i}}$$

where,

T_{i+1} = reactor mean temperature at time step i + 1, and

T_i = reactor mean temperature at time step 1.

$$\alpha_{eff,i} = \alpha_{iso,i} + \left(\frac{dP}{dT}\right)_i \alpha_p$$

where,

$\alpha_{iso,i}$ = isothermal temperature coefficient at time step i (¢/°F), and

$\left(\frac{dP}{dT}\right)_i$ = rate of change of reactor power with reactor temperature at time step i (determined from system feedback) (kw/°F).

For this study a relation of the form

$$\frac{P}{P_o} = \left(\frac{T}{T_o}\right)^n$$

was assumed.

If the radiator temperature were the same as the core temperature, the exponent n would be very close to 4.0. This arises because the heat rejection follows the T^4 radiation law and because almost all of the heat produced in the reactor is rejected to space from the radiator. Since there are temperature drops between the core and the radiator, however, n is usually less than 4.0. For thermoelectric systems, where a large temperature drop exists across the thermoelectric elements, it has been shown that n is approximately equal to 2.3 for temperatures in the range of interest for SNAP reactors. This value has been used in this study. In this case,

$$\left(\frac{dP}{dT}\right)_i = 2.3\frac{P_o T_i^{1.3}}{T_o^{2.3}} = 2.3\frac{P_i}{T_i} \quad .$$

For Mercury-Rankine systems, on the other hand, the radiator temperature is relatively constant over reasonable changes of core temperature. The exponent n is therefore close to zero. The results presented in this study are therefore strictly applicable only to thermoelectric systems. Preliminary investigations show the conclusions to hold with very minor changes for low-powered (<200 kwt) reactors in Mercury-Rankine systems. Examination of higher-powered Mercury-Rankine systems is continuing.

α_p = total power coefficient (¢/kw). This power coefficient allows for the fact that the reactor is not isothermal and for the increase in equilibrium xenon concentration with power.

$$\Delta\rho_i = \Delta HR_i - HL_i - FD_i - FP_i - \Delta PP_i$$

where,

ΔHR_i = reactivity loss over this time interval due to hydrogen redistribution,

HL_i = hydrogen leakage reactivity loss over interval i,

FD_i = fuel depletion reactivity loss over interval i,

ΔFP_i = change in fission product reactivity inventory over this interval, and

ΔPP_i = change in prepoison worth (¢) = $PP_{i+1} - PP_i$.

This prepoison burnout term is the only negative term; therefore, it contributes the only positive contribution to $\Delta\rho_i$.

The units of all the reactivity terms above are cents.

A stepwise solution of the above equation is carried out by the program. In this manner the necessary prepoison loading for a desired temperature profile is obtained.

B. REACTIVITY PENALTIES ASSOCIATED WITH THE USE OF PREPOISONS

The choice of prepoison is dependent on the application. Reactivity loss rate and power regime are most important. The poison must burn out fast enough to match the loss rate, but the rates must not significantly deviate since the result of such deviation is temperature variation. All reactivity loss mechanisms are nearly linear in time except for hydrogen leakage, which tends to decrease (assuming no barrier degradation). Since the burnout rate of a prepoison decreases as the concentration of prepoison is depleted, the rate of reactivity gain decreases more rapidly than the rate of reactivity loss when the poison supply has been nearly depleted. Studies to determine the amount of prepoison to give the best match between loss rates and gain rates have shown that a reactivity penalty of 30 to 40% of the worth of the initial prepoison loading is the general rule. Below that amount the reactivity gain rate decreases much more rapidly than the reactivity loss rate. This effect is shown by the results presented in Table 6.

TABLE 6

TIME DEPENDENCE OF PREPOISON BURNOUT

$(C = C_o\, e^{-t/\tau})$

Prepoison Concentration	Time
1.000	0
0.368	τ
0.135	2τ

Since the burnout rate must match a nearly linear loss rate, and a single exponential function is nearly linear during the first time constant, the reactivity penalty of 30 to 40% of the initial loading follows directly.

C. SNAP NEUTRON SPECTRUM

The neutron spectrum in a SNAP reactor exhibits a peak near 0.1 ev. This is a result of the moderating properties of zirconium hydride. As shown in Figure 19, for SNAP 10A, the samarium cross section exhibits a peak at very nearly the same energy. Thus a small shift (hardening) of the neutron spectrum results in a considerable decrease in the effective samarium-149 cross section. Even when the spectrum hardens, the peak remains near 0.1 ev because of the hydrogen moderator. The hardening of the neutron spectrum results in a flattening of the peak, effectively reducing the absorption rate for the poisons.

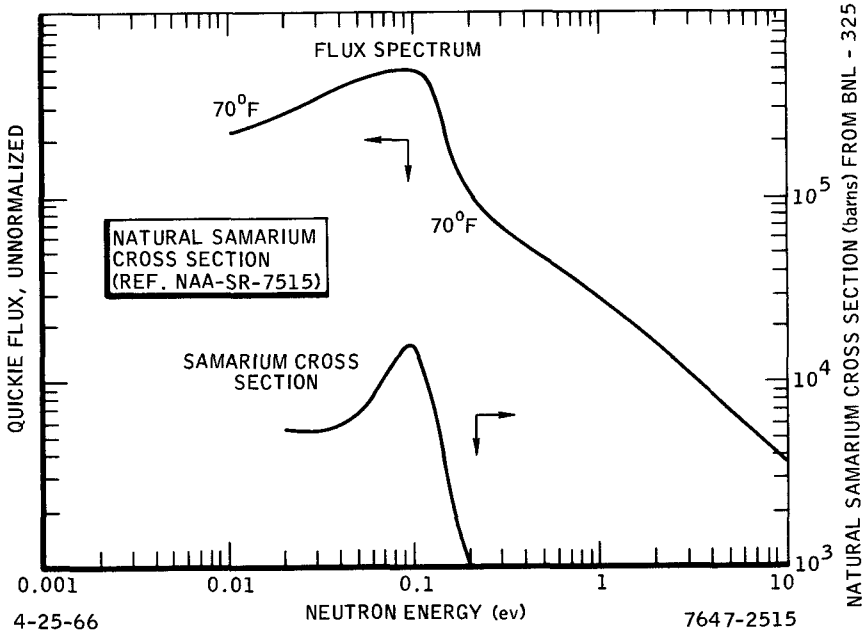

Figure 19. SNAP 10A Spectrum Calculated Using QUICKIE